University of South Bohemia in České Budějovice
Faculty of Science

Analyzing the role of p38 mitogen activated protein kinases and their effectors on mouse blastocyst maturation

Bachelor's thesis

Andrea Hauserová

Supervisor: doc. Alexander W. Bruce, Ph.D.

České Budějovice 2021

Bachelor's thesis

Hauserová A., 2021: Analyzing the role of p38 mitogen activated protein kinases and their effectors on mouse blastocyst maturation. Bc. Thesis, in English. – 49 p., Faculty of Science, University of South Bohemia, České Budějovice, Czech Republic.

Annotation

Bachelor's thesis demonstrates the role of p38 mitogen activated protein kinases and their effectors on mouse blastocyst maturation.

Prohlášení

Prohlašuji, že svoji bakalářskou práci jsem vypracovala samostatně pouze s použitím pramenů a literatury uvedených v seznamu citované literatury.

Prohlašuji, že v souladu s § 47b zákona č. 111/1998 Sb. v platném znění souhlasím se zveřejněním své bakalářské práce, a to v nezkrácené podobě elektronickou cestou ve veřejně přístupné části databáze STAG provozované Jihočeskou univerzitou v Českých Budějovicích na jejích internetových stránkách, a to se zachováním mého autorského práva k odevzdanému textu této kvalifikační práce. Souhlasím dále stím, aby toutéž elektronickou cestou byly v souladu s uvedeným ustanovením zákona č. 111/1998 Sb. zveřejněny posudky školitele a oponentů práce i záznam o průběhu a výsledku obhajoby kvalifikační práce. Rovněž souhlasím s porovnáním textu mé kvalifikační práce s databází kvalifikačních prací Theses.cz provozovanou Národním registrem vysokoškolských kvalifikačních prací a systémem na odhalování plagiátů.

V Českých Budějovicích, 13. 4. 2021 ……..

Andrea Hauserová

Acknowledgment

Above all, I would like to thank my supervisor doc. Alexander W. Bruce, Ph.D. for the opportunity to work in his laboratory and perform my bachelor research. Thanks to you, I gained valuable knowledge and important practical skills.

Secondly, I would like to express my deep and sincere gratitude to my thesis co-supervisor Pablo Bora. I would like to thank you for all of the help you have given me since my first day. I especially appreciate your patience that cannot be underestimated, guidance, enthusiastic encouragement and all of the time you have taken from your own work to help me.

Next, I would like to thank to all the members and other students of the laboratory for their kind reception, willingness to advise and help me with anything, and for the support they provided me.

Finally, I wish to thank my parents and siblings for their support and encouragement throughout my study.

Abstract

Thanks to the advantages of experimental embryology and molecular biology that have developed over the last 15 years, we have been able to study the preimplantation biology of mammals. Although there are techniques, that allow direct intervention on the genetic heritage, there are still unanswered questions that would contribute to a full understanding of the preimplantation stages of mouse embryo development. Early mammalian embryos are easily accessible to experimental manipulation due to their properties such as size and the possibility of obtaining a large number of embryos. One of the approaches to experimentally manipulate and deeper understand the basics of preimplantation development is to use antibodies to detect expression and subcellular localisation with using microscopic immuno-fluorescent staining. Among other questions, analysing the role of p38 mitogen activated kinases (p38-MAPK) and their effectors on mouse blastocyst maturation was the main. We hypothesized that p38-MAPKs have an effect on mouse blastocyst maturation, and thanks to the performed experiments and the obtained data, we confirmed the hypothesis. We have used chemical inhibition of p38-MAPK (SB220025) and compared control treated embryos and embryos upon inhibition. Results confirmed that the specific pharmacological inhibition of p38-MAPK (between E3.5-E4.5) significantly impaired the derivation of GATA4 alone expressing PrE cells by the late blastocyst stage and inhibition also results in smaller blastocyst and thus smaller blastocoel cavity. Next, factor DDX21 was identified by phosphoproteomic mass spectrometry upon p38-MAPK inhibition in the developing blastocyst. We wanted to analyze, if the function of DDX21 is influenced by p38-MAPK activity and additionally, we also decided to assay the expression of Nucleostemin (NS also known as Guanine nucleotide-binding protein-like 3 (GNL3)) protein, as it has been reported as functionally related to DDX21. We confirm that both DDX21 and NS protein levels are sensitive to p38-MAPK inhibition during blastocyst maturation, with DDX21 localisation changing from an exclusively nucleolar to a more nucleoplasmic pattern.

Key words: mouse preimplantation development, the first cell-fate decision, the second cell-fate decision, p38-MAPKs, *Ddx21*, Nucleostemin, *Tead4*.

Table of content

1 Introduction

1.1 Preimplantation development and cell fate of mouse embryos

One of the fundamental questions in developmental biology is how a multicellular organism develops from a single cell. Early embryonic development serves as a potent model to study the fundamentals of cellular and molecular mechanisms of how a single cell transforms into a multi-cellular, multi-lineage blastocyst, with distinct biological potential and function (Zernicka-Goetz et al., 2009). The preimplantation mouse embryo is an excellent model to discover how mammalian cells function in real time and *in vivo*, because it is a simple self-contained system (White et al., 2018). Early development in mouse, and indeed mammals in general, is driven by morphogenic mechanisms and starts at the moment of fertilization of a mature oocyte by sperm. After fertilization, the one-cell embryo or zygote undergoes developmentally restrictive cleavage divisions towards specification of three distinct cell lineages; the trophectoderm (TE), primitive endoderm (PrE) and the epiblast (EPI). This is the period termed as preimplantation development, during which a single cell develops and transforms into a self-contained group of blastomeres (an archaic term for early embryonic cells) enclosed by the *zona pellucida*. The resulting blastocyst stage embryo, comprising the three stated lineages, then in turn hatches from the *zona pellucida* and is ready for implantation into the uterine wall and to proceed with the post-implantation developmental stages. In figure 1, we can see a schematic depiction of preimplantation period of mouse embryo development resulting in E4.5 stage embryo with three stated lineages. The whole process of development does not require external input, but requires precise coordination that unites the haploid genomes of each parent into a single diploid genome in the zygote (White et al., 2018).

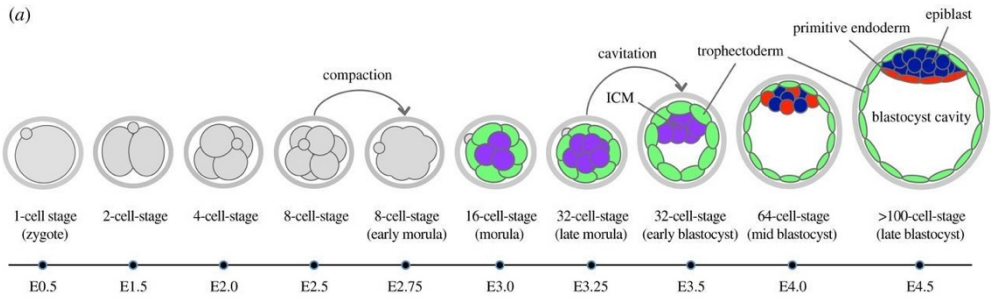

Figure 1: Schematic depiction of preimplantation period of mouse embryo development (Mihajlović & Bruce, 2017).

Primary oocytes are developmentally paused in the prophase of the first meiotic division in the ovaries of a mature female mouse and are not yet ready for fertilization. These oocytes are surrounded by support cells that provide maternal mRNAs and proteins important to sustain development through the first stages of life. After a release of luteinizing hormone from the maternal pituitary gland, sub-populations of oocytes resumes meiosis, breaks down their nuclei, and assembles a microtubule spindle around their condensed chromosomes (Bury et al., 2017). The cortex of the oocyte softens and thickens and spindle migration toward the nearest cortex is promoted (Chaigne et al., 2013). After this spindle migration, the proximity of the chromosomes to the cortex induces the formation of a critical actomyosin cap (Deng et al., 2015). Filamentous actin flows are established thanks to the formation of the actomysin cap and drive cytoplasmic streaming to maintain spindle positioning and the first polarization events (Yi et al., 2011). As such, primary oocytes become secondary oocytes after restarting and finishing the first meiotic division and a polar body containing half the original duplicated genetic content of the oocyte is formed. Subsequently, a second meiotic spindle assembles around the chromosomes and the secondary oocyte remains arrested in a stage of metaphase II arrest. It is at this point, the secondary oocyte is mature and ready for fertilization by the sperm (White et al., 2018).

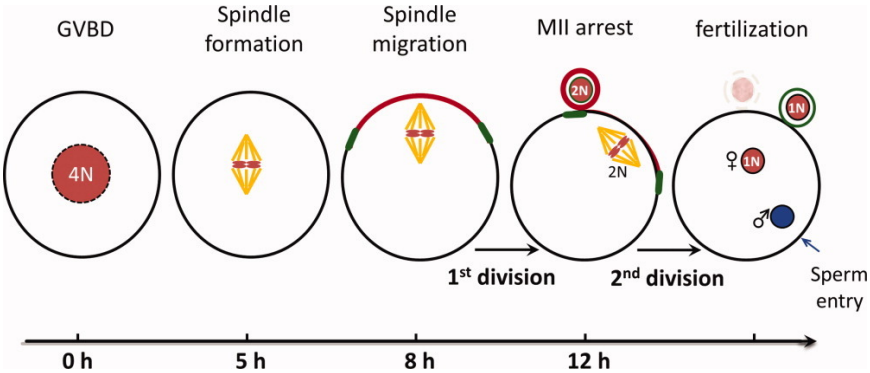

Figure 2: Schematic illustration of meiotic maturation of mouse oocytes. A prophase I arrested oocyte initiates the maturation process upon hormonal stimulation (Yi et al., 2011).

Oocyte fertilization succeeds only after ovulation, when the oocyte migrates into the fallopian tube and prepares for sperm fusion. Meiosis II resumes as a result of oocyte and sperm fusion, and during this process a second polar body is formed; consisting of a haploid complement of segregated maternal chromosomes (thus, marking the very transitory state of mature egg formation). The other remaining haploid complement of maternal chromosomes remains within the egg and together with the paternally contributed set of haploid chromosomes ensures the resulting zygote (*i.e.* fertilised egg) has a diploid genetic makeup. Secondary oocyte fertilization also prompts, formation of the maternal and paternal pro-nuclei,

maternal mRNA translation and and cell-cycle progression towards the first mitotic cell division (White et al., 2018). Early developmental progression is expressed in terms of embryonal days (E), which means the point of ovulation is set day E0 and it is approximately E0.5 is when the zygote is formed (Cockburn & Rossant, 2010). The whole process of egg maturing is described in figure 2 from (Yi et al., 2011).

A fertilized egg needs to transform to a totipotent zygote and the key for such transformation consists in nuclear remodeling enabled by several mechanisms including specific regulation of DNA methylation, post-translational histone modifications and the activation of retrotransposons. Each pronucleus, created during decondensation of the maternal and paternal chromosomes, employs a specific program for epigenetic remodeling of the parental DNA. Those programs help remove gamete-specific modifications and transform the zygote to a totipotent state (White et al., 2018).

The very early stages of preimplantation development rely on maternally provided factors, which are deposited in the egg. In mice, we can detect limited activation of zygotic transcription, termed minor zygotic genome activation (ZGA), with higher activity in the male pronucleus at the late one-cell stage. However, the majority of ZGA occurs at the two-cell stage. As development progresses from here on, the maternally supplied factors are replaced and the main regulators of development are newly synthesized embryonic products (White et al., 2018). Most of the maternally provided mRNA are actively destroyed at the two-cell embryo, but maternally provided proteins can be present during the whole of the preimplantation development (Li et al., 2013).

Up to the early eight-cell (8-cell) stage, each blastomere of the embryo is morphologically identical. We can observe the first major morphological changes during polarization and compaction at the late 8-cell stage (Figure 1). During compaction, blastomeres flatten their shape and minimize the total surface area of the embryo. E-cadherin and beta-catenin play a role in this compaction, forming adherens junction between neighboring cells, and ultimately blastocyst formation. The cell adhesion molecule E-cadherin mediates the compaction process of mouse preimplantation embryos and is also important for the function and maintenance of derived blastocyst epithelial cell layers (*i.e.* TE and PrE). For example, without the E-cadherin-encoding gene *Cdh1*, embryos are not able to form a trophectoderm (TE) epithelium or the inner cell mass (ICM) of the blastocyst (Chazaud & Yamanaka, 2016; Hyafil et al., 1980; Larue et al., 1994; Shirayoshi et al., 1983). Concomitant with compaction, 8-cell stage blastomeres also undergo the process of apical-basolateral polarization and during this process their cell contactless apical domains and cell contacted

basolateral domains are established; polarization is characterized by the differential localisation of specific protein polarity factors, differential phospho-lipid plasma membrane composition, unique F-actin domain/structures and presence or absence of microvilli between the apical and basolateral domains (Chazaud & Yamanaka, 2016).

Compaction and polarization of the embryo is followed by the segregation of resulting daughter cells into two separate populations, which will establish the first cell lineages (Mihajlović & Bruce, 2017). Each blastomere of the 8-cell embryo can be divided in one of two ways, symmetrically or asymmetrically. In the case of symmetrical divisions, both daughter cells inherit part of the contactless apical domain, resulting in two polarized cells that retain an outer position in the embryo. If a blastomere divides asymmetrically, one daughter cell inherits the apical domain and remains polar and on the outside of the embryo and the other becomes apolar and is internalized within the embryo. Similarly, outer residing 16-cell stage blastomeres can divide in one or other of these ways (Figure 1). Thus, the relative frequency of asymmetric divisions defines the proportions of the nascent outer (precursors of the TE) and inner (progenitors of the ICM) cells in the embryo by the blastocyst stage (Chazaud & Yamanaka, 2016).

At this point, the embryo consists of 16 blastomeres, that can be distinguished by their relative spatial positions in the embryo (*i.e.* as inner or outer cells). The cells that are positioned in the inner space of the embryo are apolar because they only inherited basolateral membrane and cell-cell contacts. They will form the blastocyst ICM from which the PrE and EPI lineages (representing progenitors of the extra-embryonic yolk sack and tissues of the embryonic fetus proper, respectively) will be derived. The cells on the outside of the embryo are exposed to the exterior and retain both an apical surface and basolateral membranes. These cells are polarized, and they will most likely differentiate to form the TE, from which the embryonic component of the placenta will be formed in the post-implantation developmental stages (Chazaud & Yamanaka, 2016). These patterns of structural/polarity asymmetries are critical for the expression of cell fate-specifying marker genes. One of the first major differences between the inner and outer cells is the differential activity of the Hippo-signaling pathway and downstream lineage-specifying genes. The polarized outer cells, in which the Hippo-pathway is suppressed, begin to differentiate towards the TE lineage, while conversely the apolar inner cells, in which Hippo-signalling is active, do not express differentiation factors and thus maintain pluripotency (Sasaki, 2015). This mechanism will be expanded in a later section of my thesis.

Blastocoel formation is another important step for preimplantation development. The presence of a blastocoel, a fluid-filled cavity, is essential for appropriate development of the ICM and is the defining morphological feature of the blastocyst stage embryo. The fluid-filled cavity starts to form at the 32-cell stage (around E3.5), when the outer cells have differentiated into a functional and metabolically active epithelial TE lineage. During this process of cavitation, blastomeres are spatially arranged such that the inner cells are driven to one pole of the embryo as blastocoel fluid is actively filled in to the embryonic cavity (Menchero et al., 2017). Micro-lumens emerging from the intercellular spaces within the embryo, formed by exocytosis of vesicles from basal membranes of the outer cells, cumulates towards formation of a single blastocoel cavity (Marikawa & Alarcon, 2012). A differential sodium ion concentration (driven by active transport of sodium ions across the outer cell layer through transmembrane pumps) creates an osmotic gradient and enables fluid to be pumped into the embryo cavity (Benos et al., 1985; Watson & Barcroft, 2001). Tight junctions between neighboring outer cells, forming the epithelial TE, prevents fluid leakage (H. Wang et al., 2008). According to a recent study, this permeability barrier begins with the formation of cortical actin rings on the apical surface of outer cells at the 16-cell stage (Zenker et al., 2018). These actin rings stabilize components of adherens and tight junctions. While the cavity expands, the radial symmetry of the embryo is broken and on the grounds of that, permits the separation of cell layers for the further differentiation of the ICM (White et al., 2018). Before implanting in the uterine wall, the blastocyst must hatch out of the *zona pellucida*, a protective proteinaceous shell (White et al., 2018). It has commonly been assumed that blastocyst hatching combines localized proteolytic lysis of the *zona pellucida* and mechanical pressure exerted by the expanding blastocoel cavity (Perona & Wassarman, 1986; Seshagiri et al., 2009). After emerging from the *zona pellucida*, the embryo must establish interactions with the uterus and undergo implantation to continue with successful post-implantation development (White et al., 2018).

1.1.1 The first lineage decision (trophectoderm versus inner cellular mass)

At the early stages of preimplantation development, every cell of the embryo has the potential to differentiate to any other cell type; including both the embryonic (*i.e.* fetal tissues) and extraembryonic (*i.e.* supportive tissues, such as placenta or yolk sack) lineages (Sasaki, 2015). These kinds of cells are termed totipotent, but their totipotency is restricted in mice to the zygote and each of the two blastomeres of the 2-cell stage embryo (Casser et al., 2017; Tarkowski, 1959). Individually blastomeres of the 4-cell embryo are not able to form a complete new being (Eckersley-Maslin et al., 2018; Ishiuchi & Torres-Padilla, 2013). The first

signs of differentiation between cells is most noticeable at the 16-cell stage in mouse embryos (although there is evidence for some molecular heterogeneity between 8-cell stage blastomeres, that is not fully understood), when spatial segregation of TE and ICM lineages initiates (culminating around E3.5 in the formation of the blastocyst). According to the "inside-outside model", inner and outer blastomeres of the embryo are exposed to differential cell contacts and different microenvironments from the 16-cell stage onwards, which are translated into either TE or ICM cell fate in the blastocyst. Thus, if we change the position of the cell, we can change its fate. Another model is based on the apical-basolateral polarization status of individual blastomeres and it is called the "cell polarity model." Thus, the presence or absence of cellular polarity is considered as a factor in whether it will contribute to blastocyst TE or ICM (Cockburn & Rossant, 2010). Given outer cells are typically polarized and form TE and inner cells are apolar and form ICM, it can be argued the two models are redundant. However, given experimental modulation of polarity can effect an individual blastomere's position in the embryo, and *vice-versa*, resulting in a cell fate change in the blastocyst, a unifying "cell polarity dependent positioning model" has been proposed (Mihajlović & Bruce, 2017).

A small group of transcription factor genes (TF) controls the specification of TE and ICM lineages. *Cdx2* is required for TE development and the pluripotency markers *Oct4*, *Nanog* and *Sox2* are required for establishing ICM fate. *Cdx2* is expressed at varying levels in all blastomeres starting at the 8-cell stage in the mouse and becomes restricted to the outer cells as the TE specifies and the blastocyst forms. If *Cdx2* is deleted, the TE does not develop properly and embryonic lethality is observed around the time of implantation (as the blastocyst fails to hatch). *Oct4*, *Nanog* and *Sox2*, have inverse expression patterns to that of *Cdx2*, becoming expressed only in inner cells by the blastocyst stage. After initiation, these expression patterns are reinforced by the repression of *Cdx2* gene transcription by *Oct4*, *Nanog*, *Sox2* (and *vice-versa*), along with the autoregulation of *Oct4* and *Cdx2* gene transcription (Cockburn & Rossant, 2010).

The Hippo/YAP1 signaling cascade plays a central role in TE/ICM lineage specification. It was originally found in *Drosophila* as a regulator of tissue growth. Now, it is identified as a well-conserved pathway in mammals for sensing cellular environments, such as cell density, relative cell position and stiffness of extracellular matrices (Chazaud & Yamanaka, 2016). YAP1 acts as a transcriptional co-activator of the TF TEAD4 and in mouse preimplantation embryos the TEAD4-YAP1 complex is required to transcriptionally upregulate TE-specific genes, including *Cdx2* and *Gata3* (another TF encoding gene required for TE differentiation). Differential activation of the Hippo-signalling cascade between inner and outer cells of the developing preimplantation stage mouse embryo, ensures YAP1 can complex with TEAD4 in the nuclei of outer cells (to promote TE-specific gene transcription – *e.g. Cdx2*) but is excluded from the nuclei of inner cells (to prevent inappropriate TE-specific gene expression and retain pluripotency). Thus, in the inner cells the Hippo-signalling effector kinases, LATS1/2 are activated and phosphorylate YAP1 to result in its cytoplasmic sequestration. However, as LATS1/2 is not active in outer cells, unphosphorylated YAP1 can enter the nucleus and together with TEAD4 direct TE-specific gene expression (Chazaud & Yamanaka, 2016).

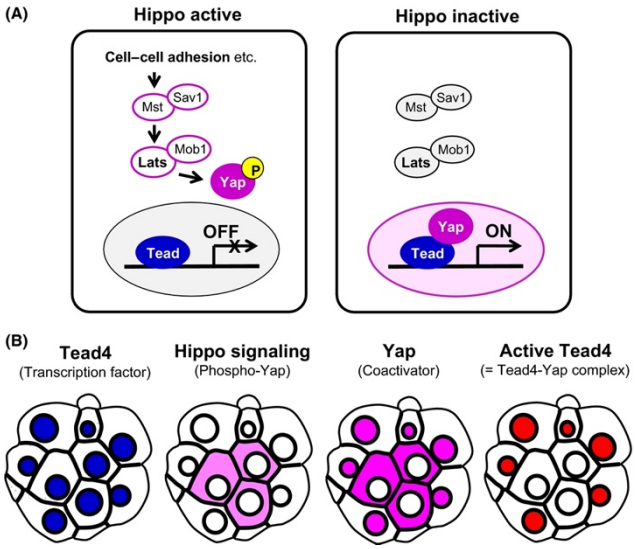

Figure 3: Schematic depiction of roles and regulations of Hippo-signaling during preimplantation mouse development (Sasaki 2017).

Figure 3 (Sasaki, 2017) shows a diagram describing the roles and regulations of Hippo signaling during preimplantation mouse development; (A) described the activation of the mouse Hippo signaling pathway, that inhibits nuclear accumulation of the coactivator protein YAP1 in apolar inner cells (left), whereas inactivation of the Hippo signaling in polarized outer cells promotes nuclear YAP1 , which activates TEAD4 directed transcription (right). (B) shows that cell position-dependent Hippo signaling controls cell fate; TEAD4 and YAP are expressed ubiquitously in all cells of the embryo but because Hippo-signaling is specifically active in, YAP1 only accumulates in the nuclei of outer cells. Active TEAD4 (*i.e.* the TEAD4-YAP1 complex) in the outer cells induces the transcription of the *Cdx2* gene. Activation of LATS1/2 requires other protein Hippo-factors. One such factor is NF2 (Merlin), a FERM domain protein. It is co-localised with LATS1/2 at all basolateral cortex/membrane sites of

both inner and outer cells and is absolutely necessary but not sufficient to activate LATS1/2 (Chazaud & Yamanaka, 2016). However, inner cell specific Hippo-signaling activation is achieved when the junction-associated scaffolding Angiomotin (AMOT) is complexed with LATS1/2 and NF2. However, this LATS1/2-NF2-AMOT complex is not formed in outer cells because the AMOT is sequestered to the apical domain, preventing formation of the active Hippo-signalling center; apical sequestration relies on specific apically enriched polarity factors and F-actin, disruption of which can release AMOT to form active Hippo-signalling centers in outer cells and block TE-specific gene expression (Hirate et al., 2013) (Chazaud & Yamanaka, 2016).

1.1.2 The second lineage decision (primitive endoderm versus epiblast)

Shortly after the act of TE and ICM specification, the ICM initiates segregation into two further lineages; the primitive endoderm (PrE) and epiblast (EPI). The embryo/fetus itself is formed from the EPI and PrE gives rise to other extraembryonic tissues (plus the gut endoderm) that are significant for further development (Cockburn & Rossant, 2010).

During the second cell-fate decision, transcription factor genes play an important role in controlling PrE/EPI specification/differentiation. *Nanog* and *Gata6* are amongst the most significant and represent the earliest expressed markers of EPI and PrE, respectively. Most, if not all, nascent ICM cells at the pre-cavitation blastocyst stage (E3.25) have yet to specify their future fate regarding the PrE and EPI lineages and actually co-express both NANOG and GATA6 proteins. However, from approximately the 32-cell stage (~E3.5 - coinciding with blastocoel cavity formation), individual ICM cells refine their expression to result in either sole NANOG or sole GATA6 expression by E4.0 (Chazaud & Yamanaka, 2016; Guo et al., 2010). This mutually exclusive ICM cell pattern of NANOG and GATA6 expression is referred to as the "salt and pepper" expression pattern and is a predictor of ultimate EPI or PrE cell fate, respectively, by E4.5; whereby the specified EPI and PrE lineages refine into their respective tissue layers by active cell movements within the ICM (and express additional genes relevant to their pluripotency or active differentiation, respectively) (Cockburn & Rossant, 2010). The mechanisms controlling the emergence of the salt and pepper pattern are considered to act through selective mRNA/protein decay, rather than via selective increases in relevant gene transcription but are also highly plastic (Chazaud & Yamanaka, 2016).

During ICM fate specification and PrE lineage differentiation, fibroblast growth factor (FGF) signaling, activating the extracellular signal-regulated kinases (ERK1/2) pathway, plays an essential role (Frankenberg et al., 2011; Kang et al., 2013). The current model for ICM cell lineage specification (see Figure 4) depends on reciprocal expression of the ligand FGF4 with refinement provided by FGFR1 and FGFR2 receptor expression (Bessonnard et al., 2014). All *Fgfr* genes (*Fgfr1-4*) are expressed in blastocyst ICM cells. *Fgfr1* is expressed in all ICM cells at all stages (*i.e.* both EPI and PrE progenitors plus EPI and PrE), *Fgfr2* is only expressed in PrE progenitors and committed PrE, whereas *Fgfr3* and *Fgfr4* are only expressed in committed PrE cells and only at the late blastocyst stage. *Fgf4* is the first gene that shows a bimodal expression distribution within the ICM at E3.25 (before cells have specified a fate choice), thereafter only being expressed in EPI-biased cells (Ohnishi et al., 2014). *Fgfr2* expression follows that of *Fgf4*, and is detected in PrE-biased cells by E3.5 (Boroviak et al., 2015; Guo et al., 2010; Ohnishi et al., 2014). Thus, the FGF4 protein extra-cellular signaling ligand is specifically only expressed by NANOG expressing EPI-fated cells (Chazaud & Yamanaka, 2016). In the absence of both *Fgfr1* and *Fgfr2* genes, maturing mouse blastocysts fail to form the GATA6 alone expressing (*i.e.* NANOG negative) PrE lineage progenitors of the salt and pepper pattern (despite initial GATA6 co-expression with NANOG) and PrE differentiation is blocked (with all ICM cells adopting an EPI fate); demonstrating that the other FGF receptors (FGFR3 or FGFR4) cannot compensate for loss of *Fgfr1* and *Fgfr2*. Interestingly, loss of the *Fgfr2* gene alone, the *Fgfr* gene specifically expressed in PrE progenitor ICM cells, does not result in drastically defective PrE differentiation (unlike sole ablation of *Fgfr1*); suggesting the existence of unique PrE- and EPI- progenitor cell mechanisms of appropriately processing the FGF4 ligand provided signal (Kang et al., 2017). Indeed, figure 4 (taken from Kang et al. 2017) argues a mechanism by which the pan-ICM expressed FGFR1 not only enables the maintenance of GATA6 levels in the PrE-biased cells (with possible refining inputs from FGFR2) but also enables the continued NANOG expression in EPI-biased cells, thus sustaining expression of FGF4 ligand to drive the segregation of EPI and PrE fated cells (Kang et al., 2017; Molotkov et al., 2017).

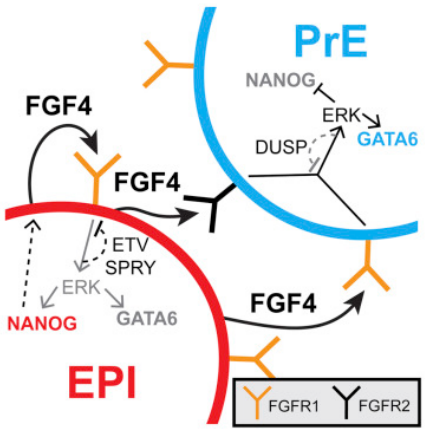

Figure 4: Expression of FGFR1 and FGFR2 in ICM EPI and PrE cells: FGF receptors FGFR1 and FGFR2 are required for PrE specification, and regulation of FGFR1 (and FGFR2) implements molecular biases between EPI and PrE cells (from Kang et al., 2017).

EPI specification is not only dependent on the TF NANOG but also on SOX2. SOX2 protein can be found in all ICM cells at E3.5 but at later stages is co-expressed with NANOG in EPI specified cells. However, the *Sox2* gene is necessary for PrE differentiation but not the initial specification of PrE progenitors by the salt and pepper stage. SOX2 promotes the process of continued PrE differentiation non cell-autonomously, via ensuring EPI-biased cells continue expressing FGF4; concomitantly it contributes to maintained expression of pluripotency genes in the ICM and eventual EPI formation (Chazaud & Yamanaka, 2016; Wicklow et al., 2014). Thus, SOX2 functions as a nodal TF by maintaining the expression of other factors, such as *Oct4* or *Fgf4* required to segregate the specified blastocyst ICM lineages. As such, *Sox2* mutant embryos are able to generate both GATA6 only and NANOG only expressing ICM cells and in the correct proportions, but the levels of GATA6 expression are lower and insufficient to drive the expression of later PrE specific genes (*e.g. Sox17* and *Gata4* (Chazaud & Yamanaka, 2016).

Therefore, in summary the specification and differentiation of PrE results from the activation of the FGF4-FGFR1/2-ERK1/2 signaling cascade, enabling sustained expression of the TF GATA6 (and downregulation of NANOG). GATA6 in turn permits expression of further PrE specific TFs, SOX17 and GATA4, to complete PrE differentiation. Note, GATA4 is expressed towards the final stage of PrE lineage establishment and does not have any effect on initial PrE specification.

1.1.3 Receptor tyrosine kinases

Receptor tyrosine kinases (RTKs) are of particular interest in the study of early embryonic development. Members of RTK family mediate vital lineage specification mechanisms during this period; the TE/ICM differentiation and segregation of the ICM to EPI and PrE (Menchero et al., 2017). RTKs are a large family of cell-surface receptors that bind extracellular factors and activate various intra-cellular signaling cascades. RTKs include the subfamilies of fibroblast growth factor receptors (FGFRs), epidermal growth factor receptors (EGFRs), vascular endothelial growth factor receptors (VEGFRs) and platelet-derived growth factor receptors (PDGFRs) and can activate various intra-cellular pathways including, the extracellular signal-regulated kinases (MAPK/ERK) and phosphatidylinositide 3-kinases (PI3K) pathway. They are involved in a broad range of cellular responses, such as embryonic development, angiogenesis, oncogenesis and regulation metabolism and stress response (Menchero et al., 2017).

As stated, RTKs, and the intra-cellular signalling cascades they activate, play important roles in the differentiation of mammalian embryonic cells. In the preimplantation stage mouse

embryo for example, one of the effectors of Ras-MAPK signaling, ERK2, is detected at the apical surface of 8-cell stage of blastomeres and is homogeneously distributed throughout all cells. Interestingly, pharmacological inhibition of ERK2 at the 8-cell stage results in a significant decrease in CDX2 protein expression, implicating Ras-MAPK (and potentially an as of yet unidentified RTK) signaling as a contributory mechanism promoting TE cell fate acquisition in the early embryo (Menchero et al., 2017). RTK based signalling is also necessary for the segregation of EPI and PrE within the ICM (as extensively discussed above in relation to FGF4-based signalling). Indeed, embryos lacking GRB2 (a RTK-associated adaptor protein) fail to differentiate PrE lineages, a phenotype shared by pharmacological inhibition of the ERK1/2 activators MEK1/2 during mouse blastocyst maturation. Interestingly, if RTK signaling is inhibited during the morula stages (compacted 8- to 32-cell), expression of GATA6 protein is not initiated (neither in the presence or absence of NANOG) in the nascent ICM at the early blastocyst stage, and the treatment reproduces the *Grb2* genetic knockout phenotype (Menchero et al., 2017). Additionally, PDGFRa mediated RTK signalling has recently been associated with promoting cell survival within the differentiated PrE lineage (Bessonnard et al., 2019; Molotkov & Soriano, 2018).

1.1.4 p38 mitogen-activated protein kinases (p38-MAPK)

p38-MAPK pathways play roles in mediating varied cellular processes, such as cell proliferation, growth, differentiation, and apoptosis. Classically, p38-MAPK pathways are characterized by their activation in response to stress-induced processes mediated by pro-inflammatory cytokines, lipopolysaccharides (LPS), ultraviolet light and various growth factors (Petersen et al., 2016). However, p38-MAPKs also play important roles during different stages of preimplantation development, and their activity is required to support development throughout that period (Bell & Watson, 2013; Bora et al., 2019, 2020; Natale et al., 2004; Thamodaran & Bruce, 2016).

The mammalian p38-MAPKs represent a subfamily of mitogen-activated protein kinases (MAPK) and comprise four isoforms encoded by different genes; p38-MAPKα (MAPK14), β (MAPK11), γ (MAPK-), and δ (MAPK13) (Natale et al., 2004). p38α was the first to be identified and represents the best characterized isoform (Remy et al., 2010). Together with the extracellular signal-regulated kinases (ERK) and c-Jun N-terminal kinases (JNK), p38-MAPKs belong to a wider superfamily of serine-threonine and tyrosine kinases. Based on the degree of amino acid sequence identity, we can divide p38-MAPK isoforms into two subsets. The first includes p38α and p38β (75% identical in mouse) and the second

comprises p38γ and p38δ (62% identical to p38α and 70% identical to each other in mouse). p38-MAPKs are activated via phosphorylation by the MAPK kinases, MKK3 and MKK6. MKK3 and MKK6 are essential for the activation of p38β and p38γ caused by environmental stress, whereas MKK6 phosphorylates and activates p38γ by responding to the cytokine tumor necrosis factor-α (TNFα) and MKK3 activates p38δ upon exposure to UV radiation (Remy et al., 2010). These are the classically defined canonical pathways, but it is hypothesized there may be many factors that can cross-talk and activate these MAPK kinases or potentially p38-MAPKs directly. Activated p38-MAPKs themselves are estimated to be able to phosphorylate and regulate around 200-300 varied downstream substrate/targets, including other regulatory kinases, transcriptional factors and chromatin remodelers (Cuadrado & Nebreda, 2010).

All four members of the p38-MAPK family are expressed during the mouse embryo preimplantation development period. p38-MAPK activity is required at the 8-cell stage to promote development to the blastocyst stage (Remy et al., 2010). To analyze the role of p38-MAPK in mouse preimplantation development, one effective method is pharmacologically inhibition. Inhibition of p38-MAPK activity prior to blastocoel cavity formation (between E1.5 to E3.5) results in reversible developmental arrest around morula stage with no or deformed cavity formation, indicating p38-MAPK activity is required for successful preimplantation development. p38-MAPK is also a potent regulator of filamentous actin around the 8-cell stage and can thus impact embryo compaction (Natale et al., 2004). The p38-MAPK pathway is not only required for blastocyst cavity formation but is implicated in facilitating TE tight junction formation and function and sustaining blastocoel expansion required for embryo hatching (Giannatselis et al., 2011; McLaren & Smith, 1977); pharmacological p38-MAPK inhibition experiments also reveal aquaporin (AQP3) and Na/K+ ATPase dysregulation (Bell & Watson, 2013). Work from our laboratory has shown p38-MAPK activity between E3.5 and E4.5 is also necessary for proper PrE specification and differentiation, but not EPI specification/formation (Thamodaran & Bruce, 2016). In subsequent works we have also reported evidence that p38-MAPK is required to ameliorate amino acid deprivation induced oxidative stress, and resultant blastocyst developmental defects, by enabling increased antioxidant enzyme gene expression (Bora et al., 2019). The latest work from our laboratory has uncovered more of the mechanistic basis of the role of p38-MAPK in blastocyst PrE lineage specification and differentiation. This work demonstrates p38-MAPK is a regulator of multiple ribosome biogenesis associated factors, rRNA processing and general protein translation during an early window of blastocyst maturation (E3.5 to E4.5) required to prime PrE specification and subsequent differentiation

(Bora et al., 2020). Having contributed towards this aforementioned manuscript (currently available as a preprint but also in the latter stages of revision after peer-review - *Communications Biology*), part of the observations in that manuscript are expanded upon in the *Results* section of this thesis. Furthermore, using phosphoproteomic mass spectrometric analysis, we identified potential effectors of p38-MAPK, of which MYBBP1A was experimentally verified to be necessary in early embryonic development and PrE specification/differentiation (Bora et al., 2020). A second factor, DDX21, was also identified in one of our p38-MAPK related mass spectrometric screens, and given its functional association with MYBBP1A, we have explored its role further (Bora et al., 2021 – *manuscript in preparation*); the bulk of this thesis is dedicated to experiments contributing to this second manuscript.

1.1.5 DEVD subfamily protein RHII/Guα gene (*Ddx21*)

The protein RHII/Guα of the DEVD subfamily, encoded in mice by the *Ddx21* gene, is a member of the DExD/H family. The DExD/H box family of proteins function as ATP-dependent RNA helicases and are known to play important roles in all aspects of RNA synthesis and function (from pre-mRNA processing, ribosome biogenesis, RNA turnover, RNA export, mRNA translation and modulation of complex RNA containing structures). According to the literature review of Fuller-Pace (Fuller-Pace, 2006), there is evidence that several members of the DExD/H family of proteins have multiple cellular functions that are independent of their RNA helicase activity. The DExD/H box proteins have considerable sequence and structural homology within their conserved helicase core but importantly they have flanking N- and C-terminal domains that are highly divergent and thought to provide substrate specificity (in terms of both RNA and protein interactors). There is also evidence suggesting some DExD/H box proteins play important roles in transcriptional regulation (Fuller-Pace, 2006).

RHII/Guα (hereon referred to as DDX21) was first identified as a nucleolar protein recognized by an auto-immune anti-sera derived from a patient with "watermelon stomach disease". It was later determined as an interacting partner for c-Jun, from a tandem affinity purification/mass spectrometric analysis, whereby the C-terminal domain of DDX21 interacts with the N-terminal transactivation domain of c-Jun (a key transcription factor involved in cellular response to stress, apoptotic and differentiation signals). Moreover, overexpression of ATPase/helicase defective DDX21 mutants or the intra-cellular microinjection of anti-DDX21 antibodies can inhibit c-Jun mediated transcriptional activation, *in vitro* (Fuller-Pace, 2006).

Additionally, it has been reported that DDX21 is required for processing of 20S rRNA to the 18S form incorporated into ribosomes (Fuller-Pace, 2006). Indeed, the DDX21 protein has been more recently implicated in the regulation of the two transcriptional arms of ribosome biogenesis, synthesis and processing of the rRNA in the nucleolus and transcription of ribosomal protein coding genes in the nucleoplasm (Calo et al., 2015). Moreover, nucleolar stress induced by inhibition of RNA polymerase I (Pol I) causes re-localization of DDX21 from the nucleolus to the nucleoplasm and simultaneous loss of DDX21 protein from Pol I and RNA polymerase II (Pol II) target gene promoters (Calo et al., 2015). DDX21 protein also biochemically co-fractionates with the pre-60S ribosomal subunit, along with other rRNA processing proteins such as Pescadillo homolog (PES1), Eukaryotic translation initiation factor 4E-binding protein 2 (EIF4EBP2) and Guanine nucleotide-binding protein-like 3 (GNL3; aka Nucleostemin/NS) (Romanova et al., 2009). In Bora *et al.,* 2021 (*manuscript in preparation*) we plan to report the first observations of DDX21 protein expression and sub-cellular localisation during preimplantation embryonic development; from E1.5 (2-cell stage) to E4.5 (late-blastocyst). The expression of *Ddx21* mRNA transcripts in developing mouse preimplantation embryos has been found (in published global mRNA screens) to initiate around 2-4 cell stage, peak at 8-cell stage and remain highly expressed throughout and in all blastocyst lineages thereafter; with close to nil expression in the maturing oocyte (Wang et al., 2018; Zhang et al., 2016). Consequently, DDX21 protein expression is not of maternal origin and is derived from transcripts expressed as a result of ZGA (Bora et al., 2021 - *manuscript in preparation*).

2 Thesis aims

- Measurement and comparison of blastocoel cavity volume with and without p38-MAPK inhibition.
- Quantification and analysis of potential p38-MAPK effector expression (DDX21 and NS) during blastocyst maturation ± p38-MAPK inhibition, using immuno-fluorescence staining confocal microscopy.
- Measurement and comparison of blastocyst cavity volume upon clonal RNAi mediated knockdown of the candidate p38-MAPK effector *Ddx21*in blastocysts, versus controls.
- Measurement and comparison of blastocyst cavity volume upon clonal RNAi mediated knockdown of the *Tead4* gene, versus controls.

3 Materials and methods

3.1 Mouse lines and embryo culture

All experiments performed on mice were carried out in accordance with EU directive 2010/63/EU. F1 hybrid female mice (derived from C57BL6/J (female) x CBA/W (male) cross) were super-ovulated by peritoneal injection with 7.5 IU PMSG (pregnant mare serum gonadotrophin extract; Folligon® MSD Animal Health) and 48 hours later with 7.5 IU hCG (human chorionic gonadotrophic hormone; Sigma-Aldrich® cat. #CG10) and transferred into a cage with one F1 male to mate overnight. Approximately 42 hours after hCG injection females were killed by cervical dislocation and the fallopian tubes immediately transferred into M2 media (pre-warmed at 37°C for at least 2-3 hours). 2-cell stage embryos (E1.5) were isolated in M2 media and cultured in KSOM media (EmbryoMax® KSOM Mouse Embryo Media; cat. #MR-020P-5F – pre-warmed and equilibrated in 5% CO_2 and 37°C) with amino acid (AA) supplementation (KSOM +AA; Gibco MEM Non-Essential Amino Acids Solution (100x) used at a working concentration of 1x, cat. #11140035 and Gibco MEM Amino Acids Solution (50×) used at a working concentration of 0.5x, cat. # 11130036) Embryos were cultured in KSOM+AA micro-drops (approx. 15µl) prepared in 35mm tissue culture dishes, overlaid with light mineral oil (Irvine Scientific. Cat. #9305) and maintained in 5% CO_2 incubators at 37°C until the appropriate stage.

3.1.1 Embryo culture under chemical inhibition

Embryos with a blastocoel cavity that occupied approximately 50% of the embryo's volume at E3.5 were moved to either inhibitory or control culture conditions and cultured for a further 24 hours (to the E4.5 stage). Inhibition of p38-MAPK was performed using SB220025 (Calbiochem® cat. #559396; dissolved in dimethyl sulfoxide/DMSO) at 20µM working concentration in KSOM+AA culture medium; an equivalent volume of DMSO solvent was used in the control culture conditions.

3.2 Fixing and immunofluorescence staining

After the required *in vitro* cultivation period, embryos were quickly washed in fresh and pre-warmed KSOM+AA and pipetted into pre-warmed drops of acid Tyrode's Solution (Sigma-Aldrich® cat. #T1788) to remove the *zona pellucida*. After *zona pellucida* was no longer visible, embryos were immediately washed through pre-warmed drops of M2 media and fixed with 4% paraformaldehyde (Santa Cruz Biotechnology, Inc. cat. # sc-281692) for 15 minutes at room temperature. Embryos were then washed in 3 drops of PBS containing 0.05% TWEEN® 20 (PBST; Sigma-Aldrich cat. #P9416) for 20 minutes. Embryos were

transferred to a 0.5% solution of Triton X-100 (Sigma-Aldrich® cat. #T8787), in phosphate buffered saline (PBS), to permeabilize for 20 minutes at a room temperature. Embryos were then washed again in 3 drops of PBST for 20 minutes. Blocking was performed in 3% bovine serum albumin (BSA; Sigma-Aldrich® cat. #A7906) in PBST for 30 minutes at 4°C, followed by primary antibody incubation (at the desired dilution in blocking buffer) overnight at 4°C. Embryos were then washed in 3 drops of PBST for 20 minutes and blocked for 30 minutes at room temperature. Suitably diluted (in blocking buffer) fluorescently conjugated secondary antibodies were then used to stain the embryos by room temperature incubation for 70 minutes. The immuno-fluorescently stained embryos were then mounted in DAPI-containing VECTASHILED® medium (Vector Laboratories, Inc. cat. #H-1200), placed under cover slips on glass-bottomed 35mm culture plates and incubated at 4°C for 30 minutes in the dark, prior to fluorescent confocal microscopy mediated image acquisition. The details of the primary and secondary antibodies used and their dilutions/concentrations are summarized in table 1.

Tab. 1: An overview of used antibody and their dilution

Antibody against	Type	Target	Host/Isotype	Manufacturer	Dilution used
NANOG	Primary (monoclonal)	Mouse	Rat / IgG2a	Thermo Fisher (14-5761-80)	1:200 in PBST (3% BSA)
GATA-4	Primary (polyclonal)	Mouse, rat and human	Rabbit / IgG	Santa Cruz Bio. (sc-9053)	1:200 in PBST (3% BSA)
CDX2 (CDX2-88)	Primary (monoclonal)	Conserved	Mouse / IgG1, kappa	BioGenex (MU392A-5UC)	1:200 in PBST (3% BSA)
DDX21	Primary (polyclonal)	Conserved	Rabbit / IgG	Novus (NB100-1718)	1:100 in PBST (3% BSA)
NUCLEOSTEMIN (quantification of available images only)	Primary (monoclonal)	Mouse, rat and human	Mouse / IgG1, kappa	Santa Cruz Bio. (sc-398978)	1:100 in PBST (3% BSA)
Donkey anti-Rat IgG (H+L) Highly Cross-Adsorbed Secondary Antibody, Alexa Fluor 488	Secondary (polyclonal)	Rat	Donkey / IgG	Thermo Fisher (A-21208)	1:500 in PBST (3% BSA)
Donkey anti-Rabbit IgG (H+L) Highly Cross-Adsorbed Secondary Antibody, Alexa Fluor 555	Secondary (polyclonal)	Rabbit	Donkey / IgG	Thermo Fisher (A-31572)	1:500 in PBST (3% BSA)
Donkey Anti-Rabbit IgG H&L (Alexa Fluor® 647)	Secondary (polyclonal)	Rabbit	Donkey / IgG	Abcam (ab150075)	1:500 in PBST (3% BSA)
Donkey anti-Mouse IgG (H+L) Highly Cross-Adsorbed Secondary Antibody, Alexa Fluor 488	Secondary (polyclonal)	Mouse	Donkey / IgG	Thermo Fisher (A-21202)	1:500 in PBST (3% BSA)

Embryos cultured in both p38-MAPK inhibited and control conditions were immuno-fluorescently stained by a combination of two primary antibodies and respective secondary antibodies as required for specific experiments (Table 2).

Tab. 2: An overview of used antibody combinations:

Antibody combinations used				
	Primary 1	Primary 2	Secondary to primary 1	Secondary to primary 2
1	NANOG (rat)	GATA4 (rabbit)	Donkey α rat 488	Donkey α rabbit 555
2	NANOG (rat)	GATA4 (rabbit)	Donkey α rat 488	Donkey α rabbit 647
3	CDX2 (mouse)	DDX21 (rabbit)	Donkey α mouse 488	Donkey α rabbit 647
4	NUCLEOSTEMIN (mouse)	DDX21 (rabbit)	Donkey α mouse 488	Donkey α rabbit 647

3.3 Confocal microscopy

Glass-bottomed culture plates with fixed and fluorescently immuno-stained embryos were placed on the stage of a FV10i Confocal Laser Scanning Microscope, using FV10i-SW image acquisition software (Olympus®). Embryos were imaged in 3D in a series of z-stacks with step-size of 2µm (for example, an approximately 100µm diameter spherical blastocyst embryo at E4.5 will be imaged in 51 stacks). Embryo images were analysed using FV10-ASW 4.2 Viewer software (Olympus®).

3.4 Cell number quantification and statistical analysis

Total number of cells per embryo were quantified on the basis of pan-nuclear DAPI staining. In experiments to visualize ICM lineages, inner cells were divided into two groups based on sole detectable NANOG or GATA4 immunofluorescence (representing EPI and PrE, respectively). Cells which did not stain for either GATA4 or NANOG and also did not reside within the blastocyst ICM, were determined as outer/TE cells. ICM cells positively stained for both GATA4 and NANOG were classified as neither PrE or EPI (and recorded – likewise numbers of ICM cells staining for neither protein marker). In experiments analysing DDX21 expression, embryos were co-stained with anti-CDX2 antibody, to differentiate between outer (expressing CDX2) and inner (not expressing CDX2) cells. Regarding, the analysis of embryos co-stained for NUCLEOSTEMIN and DDX21 expression, individual cells were differentiated into inner and outer populations based only upon a judgement of their physical location in the embryo. Counting of the total number of cells in each category were carried out manually using ImageJ (Fiji) software and data accumulation/record keeping using Microsoft Excel; further statistical analysis and chart preparation was performed using GraphPad.

3.5 Fluorescence intensity quantification

Fluorescence intensity was quantified for the minimal complete confocal z-series of each embryo using Fiji (ImageJ) software. Levels of DDX21 were quantified as fluorescence intensity per cell nucleus and differentiated into inner and outer cell populations (as described

above). The measurement settings were as follows: Analyze>Set Measurements; and the following options were chosen: Area, Mean grey value and Integrated density. An area encompassing the nucleus (based on DAPI staining) was marked off using the "Polygon selections" tool and the measurements were recorded. The selected area was then moved to comprise an area excluding that of the embryo or cell nucleus, and correcting background measurements recorded. This process was repeated for all the embryos analysed, under both control and p38-MAPK inhibited conditions and the results were recorded on Excel sheets for further analyses. The Corrected Total Cell Fluorescence (CTCF), in arbitrary units (au), for each embryo was measured as such: CTCF = Integrated Density – (Area of selected cell X Mean fluorescence of background readings) (McCloy et al., 2014; Potapova et al., 2011).

3.6 Blastocyst size and volume calculations

The volume of blastocoel cavities was calculated by measuring their inner circumference, whereas the volume of the total blastocyst embryo as a whole was calculated by measuring the outer circumference of the entire blastocyst; both employing the centrally located widest/equatorial z-slice image, using Fiji (ImageJ) software. The settings used in the Fiji program were as follows: Analyze>Set Measurements; with the "Perimeter" option selected, the "Polygon selection" tool was used mark the required circumferences. The radii of the measured circumferences were mathematically derived and used to calculate an approximate volume for all embryos analysed. The calculated volume in picolitres (pL) was plotted as a scatter, representing the complete assayed embryo population, with mean and standard deviations (SD) marked.

3.7 Statistical analysis

Statistical analysis was carried out using GraphPad Prism. The specific tests used were determined by tests for Gaussian distribution of the respective dataset. Datasets with normal distribution were compared by using unpaired two-tailed t-test and datasets with log-normal distribution were compared using Mann-Whitney tests (specified within respective data analysis figures). In one case (for comparison of NANOG & GATA4 co-positive cell numbers between DMSO and p38-MAPKi conditions) a t-test was combined with Welch's correction for unequal SD. Respective p-values arising from the statistical tests are plotted within the graphs and the degree of significance determined as such (Table 3):

Tab. 3: Degree of significance

P value	Wording	Summary
< 0.0001	Extremely significant	****
0.0001 to 0.001	Extremely significant	***
0.001 to 0.01	Very significant	**
0.01 to 0.05	Significant	*
≥ 0.05	Not significant	ns

Some of the data analysed in this thesis are from experiments carried out by other members of the laboratory and are as follows: Initial immunofluorescence microscopy for NUCLEOSTEMIN in control vs. p38-MAPKi conditions; *Ddx21* downregulation by microinjection of *Ddx21* siRNA into 2-cell stage preimplantation embryo was performed by Pablo Bora (result reported in section 4.4); *Tead4* downregulation by microinjection of *Tead4* siRNA into 2-cell stage preimplantation embryo was performed by Rebecca Collier (result reported in section 4.5).

4 Results

4.1 p38-MAPK inhibition between E3.5 and E4.5 results in PrE cell fate defects

As part of our laboratories manuscript investigating the mechanisms of p38-MAPK inhibition (related to regulation of protein translation) induced defects in PrE specification and differentiation (between E3.5-E4.5), we wanted to investigate the average size of blastocyst cavities in p38-MAPK inhibited embryos versus controls (Bora et al., 2020). This was because a recently reported study suggested impaired cavity expansion negatively affected ICM lineage derivation and particularly PrE formation (Ryan et al., 2019). Therefore, we culture E3.5 stage mouse embryos under both control (+DMSO) and p38-MAPK inhibited (+SB220025) conditions until the late blastocyst stage (E4.5). Embryos were then fixed and immuno-fluorescently stained for NANOG and GATA4 protein expression and subsequently complete z-series confocal sections per embryo were acquired by confocal microscopy. Before, making measurements of blastocyst cavity volume, we first calculated the average total, inner and outer cell number per group and the number of NANOG and GATA4 expressing ICM cells. This was to ensure we observed the same specific p38-MAPK inhibition induced deficit in PrE differentiation (without affecting specification of the EPI) as we previously reported; thus, providing the necessary reassurance of the efficacy of the p38-MAPKi inhibitor before calculating the potentially correlating cavity volumes. Figure 5 shows representative micrographs of blastocysts from the control/DMSO and p38-MAPK inhibited/SB22025 treated groups.

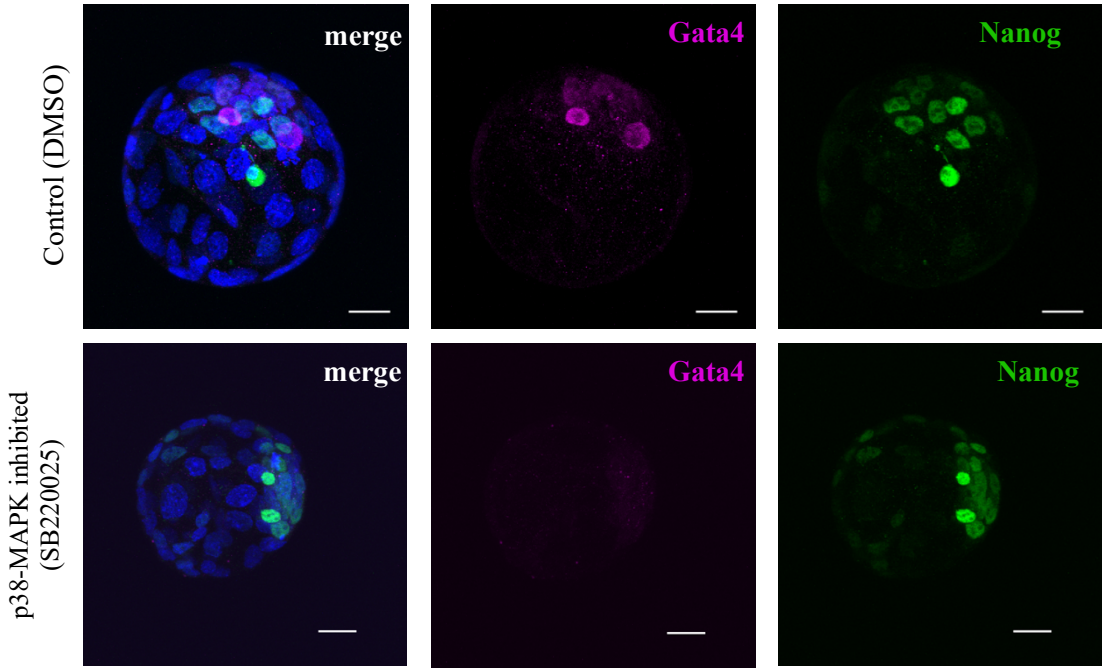

Figure 5: Representative projected z-stack confocal images of blastocysts treated (between E3.5-E4.5) with DMSO control (upper row) or SB220025 p38-MAPK inhibitor (lower row), fixed and immuno-stained for EPI marker NANOG (green) and PrE marker GATA4 (magenta) at E4.5. DNA DAPI counterstain (blue) is shown in merged image; scale bar represents 20μm.

As can be seen in Figure 5, p38-MAPK inhibition appeared to be associated with highly reduced GATA4 expressing ICM cells (or an absence in the example shown – Figure 5) and continued expression of NANOG. These data strongly suggested the employed p38-MAPKi inhibition regime was recapitulating our previously reported block in PrE specification and differentiation (Bora et al., 2019; Thamodaran & Bruce, 2016). This interpretation was supported by the results of our cell counting analyses. As can be seen in Figures 6, 7 and 8, there were no significant differences in total (73.10 versus 68.38), outer (56.21 versus 53.43) and inner (16.9 versus 14.95) cell number between control and p38-MAPK inhibited blastocyst groups; indicating the p38-MAPK inhibitor (SB220025) was not cytotoxic.

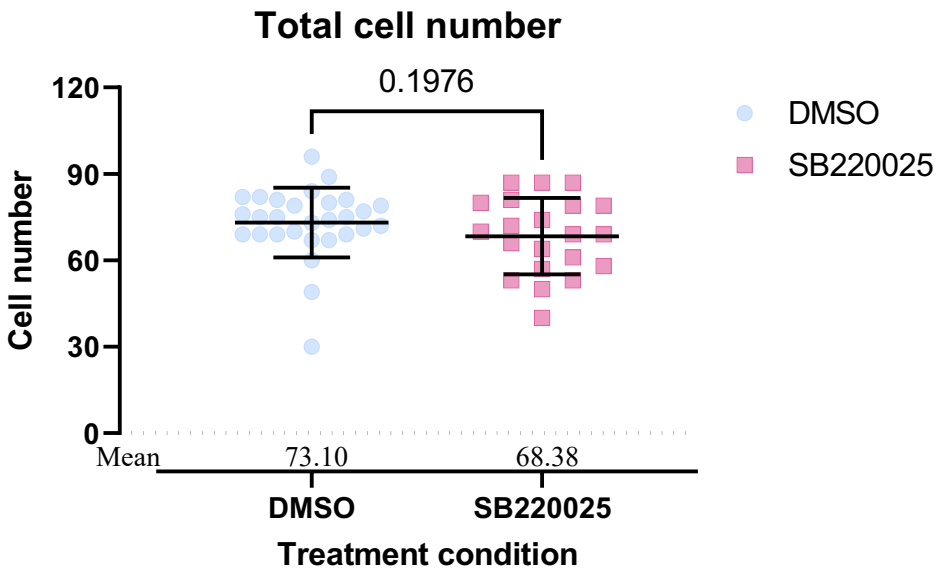

Figure 6: Graph showing a comparison in the average total cell number of control treated (DMSO - n=29) and p38-MAPK inhibited (SB220025 - n=21) embryos (between E3.5-E4.5) as measured at E4.5. Errors are represented as standard deviations and a statistical unpaired t-test was used; p-value stated (0.1976) ns.

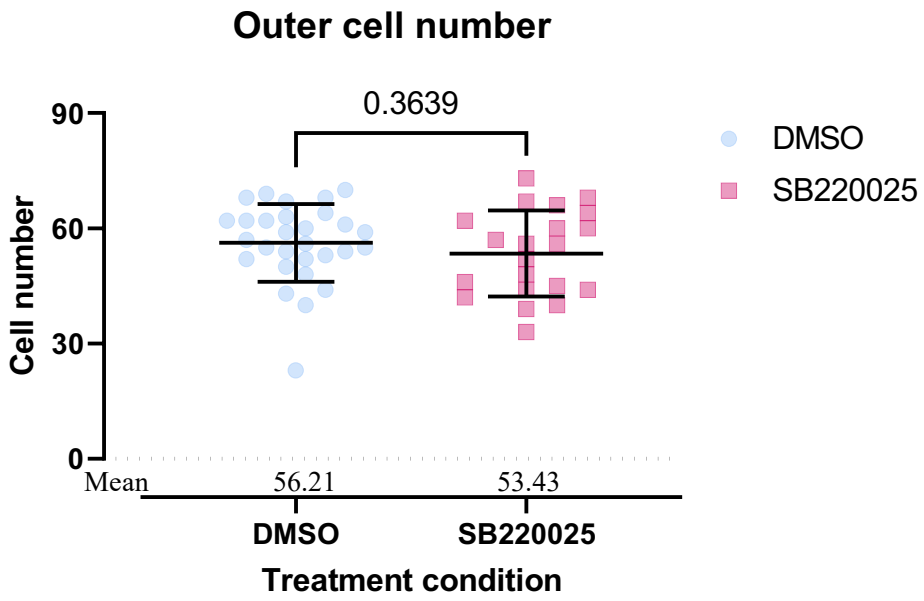

Figure 7: Graph showing comparison of outer cell number of control treated embryos and inhibited embryos (SB220025). Errors are represented as standard deviations and statistical unpaired t-test was used; p-value stated (0.3639) ns.

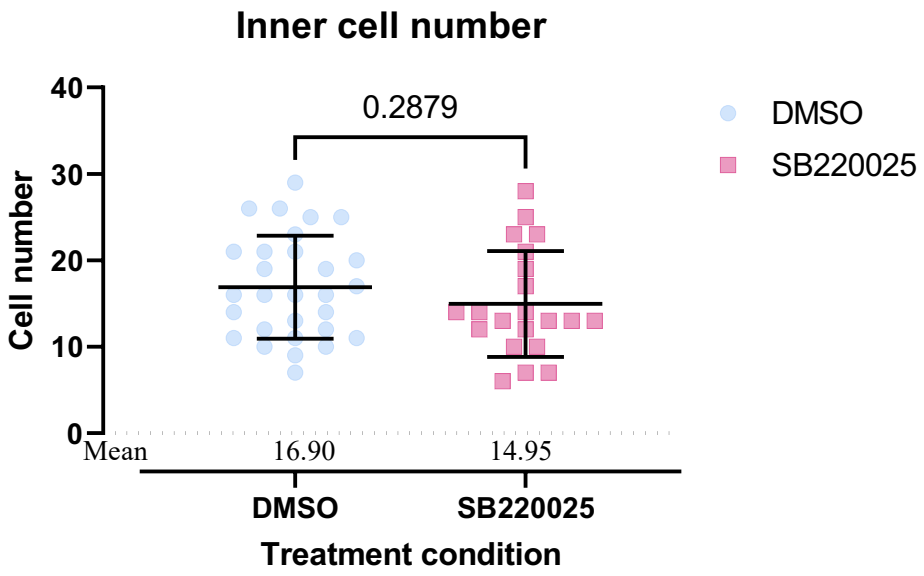

Figure 8: Graph showing comparison of inner cell number of control treated embryos and inhibited embryos (SB220025). Errors are represented as standard deviations and statistical Mann-Whitney test was used; p-value stated (0.2879) ns.

We next counted the number of ICM cells expressing the late blastocyst lineage markers, NANOG (EPI) and GATA4 (PrE - Figures 9-12). The number of ICM cells solely expressing NANOG in p38-MAPK inhibited blastocyst was found to be slightly elevated versus controls, although this was not statistically significant (11.52 versus 10.72, respectively – Figure 9). However, the number of ICM cells expressing GATA4 only, indicative of PrE differentiation, was significantly and markedly reduced (3.00 versus 5.48, respectively – Figure 10). The number of ICM cells co-expressing both NANOG and GATA4 was negligible and insignificantly different in both conditions (0.69 versus 0.43 – Figure 11); presumably reflecting the fact PrE differentiation (as determined by GATA4 expression) ordinarily requires down regulation of NANOG protein levels (as revealed in the salt and pepper pattern during normal blastocyst maturation). Collectively, these data confirm the p38-MAPK inhibition regime employed during blastocyst maturation (E3.5-E4.5) was effective at impairing PrE formation. This is further illustrated by the significantly reduced ratio of GATA4 positive expressing PrE cells, as normalized to average total ICM cell number in p38-MAPK inhibited blastocyst (0.18 versus 0.33 – Figure 12).

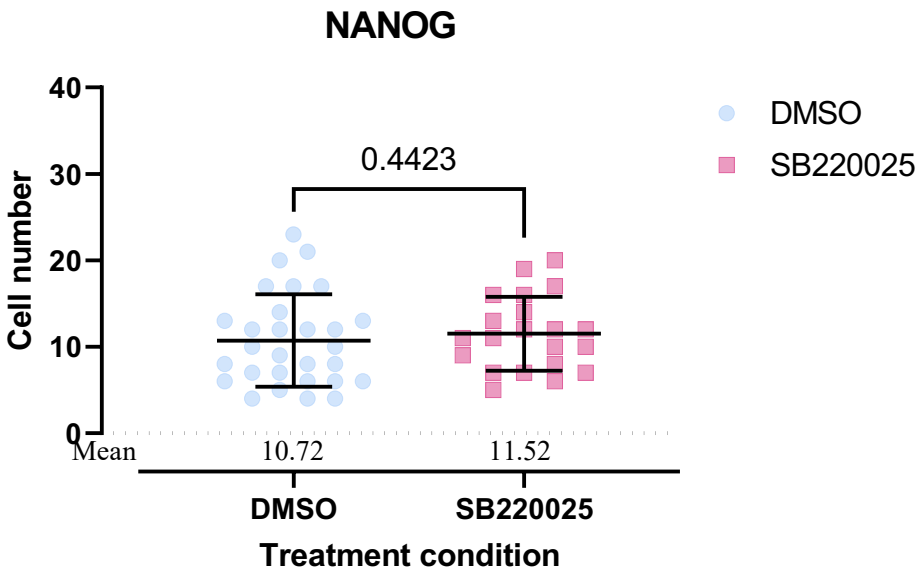

Figure 9: Graph showing cell number of Nanog positive cells of control treated embryos (DMSO) and inhibited embryos (SB220025). Errors are represented as standard deviations and statistical Mann-Whitney test was used; p-value stated (0.4423) ns.

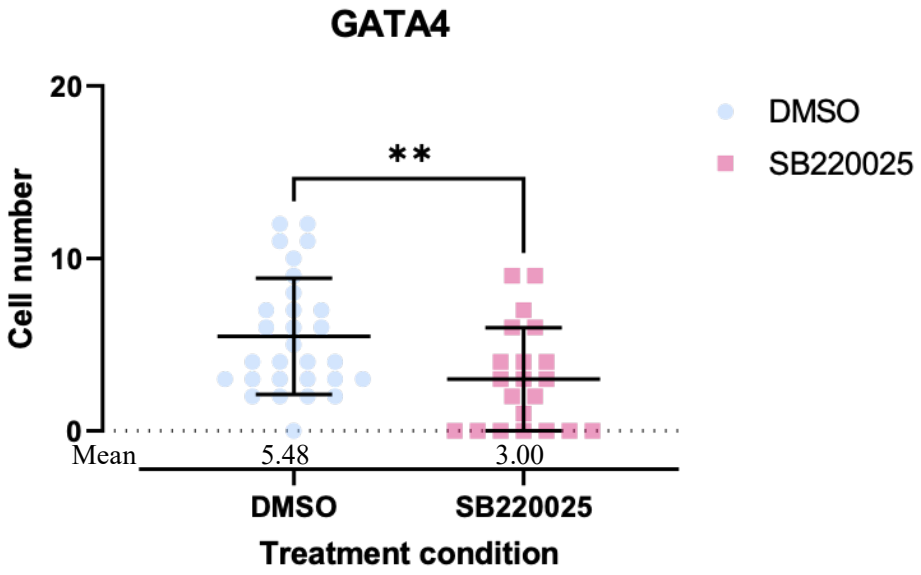

Figure 10: Graph showing cell number of GATA4 positive cells of control treated embryos (DMSO) and inhibited embryos (SB220025). Errors are represented as standard deviations and statistical unpaired t-test was used; p-value stated (0.0096) **.

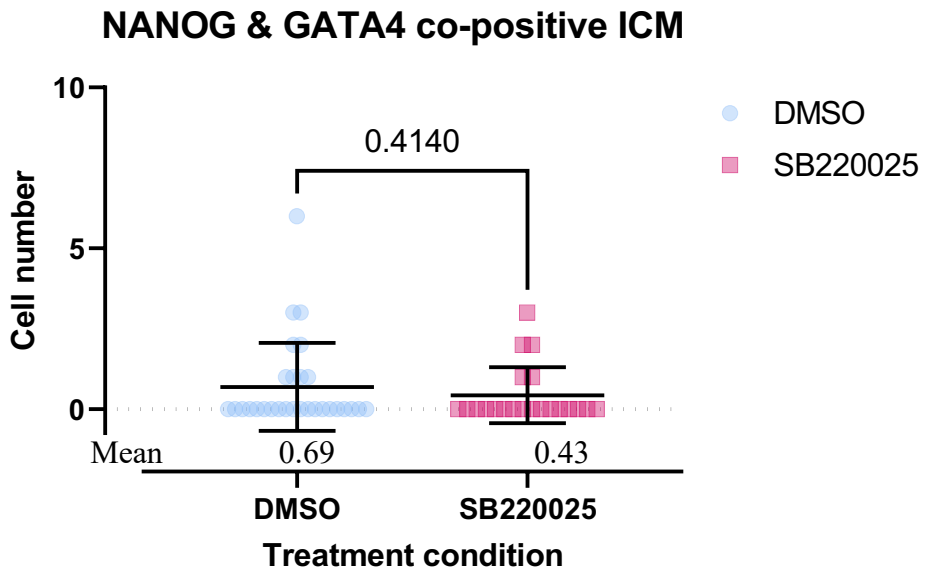

Figure 11: Graph showing cell number of NANOG and GATA4 co-positive cells of ICM of control treated embryos (DMSO) and inhibited embryos (SB220025). Errors are represented as standard deviations and statistical unpaired t-test with Welch's correction was used; p-value stated (0.4140) ns.

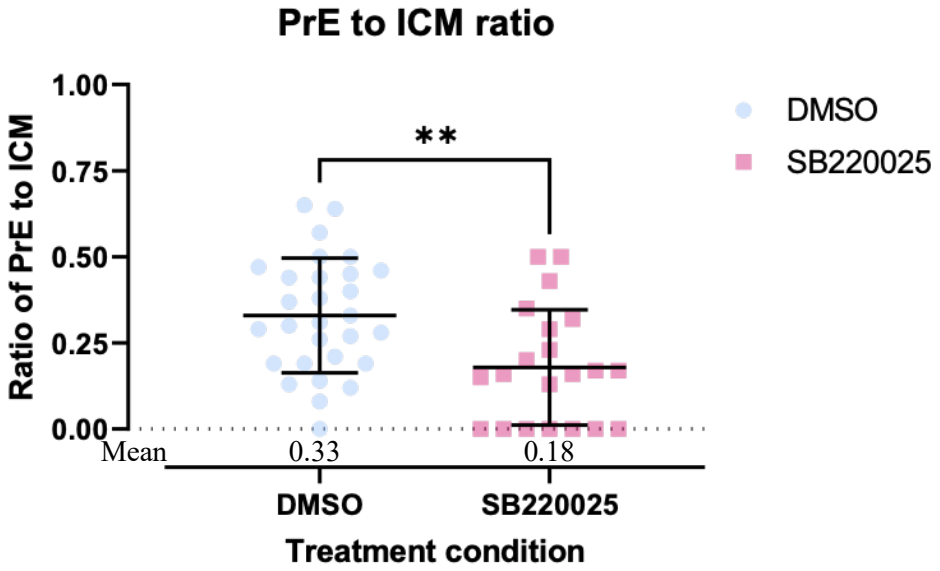

Figure 12: Graph showing ratio of PrE to ICM of control treated embryos (DMSO) and inhibited embryos (SB220025). Errors are represented as standard deviations and unpaired t-test was used; p-value stated (0.0028) **.

Overall, these results confirmed the specific pharmacological inhibition of p38-MAPK (between E3.5-E4.5) significantly impaired the derivation of GATA4 alone expressing PrE cells by the late blastocyst stage. Thereby, providing the required confidence to assay for correlative differences in the average blastocyst cavity volumes of each treatment group.

4.2 p38-MAPK influences blastocoel cavity expansion

Having confirmed the efficacy of the p38-MAPK inhibition treatment to cause the previously described defective PrE phenotypes, we next measured the average blastocyst cavity volumes (pL) in the same control and p38-MAPK inhibitor treated blastocysts (Figure 13). We found that as predicted, p38-MAPK inhibited blastocysts presented with a highly and significantly reduced cavity volume (162.9 pL versus 384 pL in controls – Figure 13). We therefore conclude that PrE differentiation phenotypes observed in the maturing mouse blastocyst ICM under p38-MAPK inhibited conditions are also associated with reduced blastocyst cavity expansion. These data strongly agree with observations from another group that correlate ICM lineage specification (particularly PrE) and blastocoel expansion (Ryan et al., 2019). Moreover, they have been included into our laboratory's the recent paper mechanistically assaying the role of p38-MAPK (focusing on protein translation regulation) during the early phase of mouse blastocyst maturation (Bora et al., 2020).

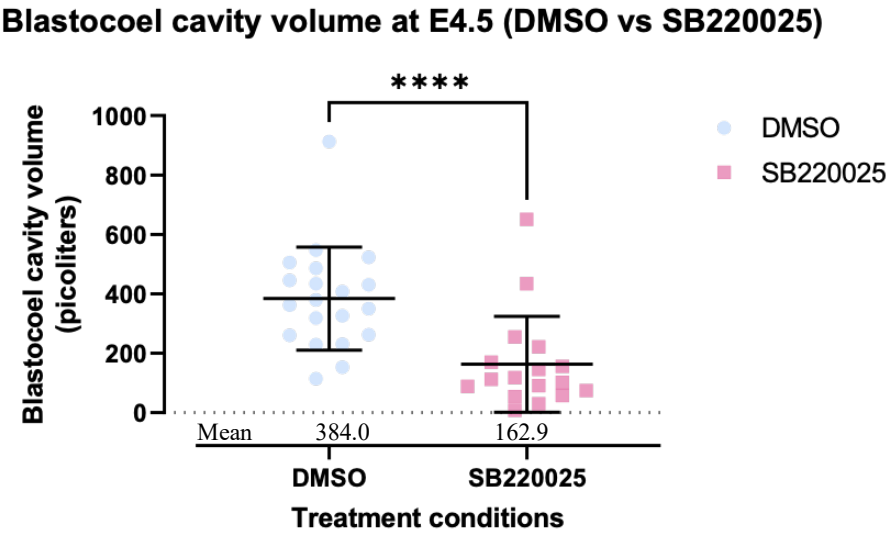

Figure 13: Mean blastocoel cavity volumes (pL) of E4.5 stage blastocysts treated with control DMSO (n=20) or SB220025 p38-MAPK inhibitor (n=17) between E3.5-E4. Errors are standard deviations. Mann-Whitney test was used in statistical analysis of significance.

4.3 DDX21, a potential p38-MAPK effector, shows an intra-cellular shift in localization during preimplantation development

As referenced above, previous studies from our group have confirmed and begun to mechanistically resolve the significant role of p38-MAPK in blastocyst maturation and PrE specification (Bora et al., 2019, 2020; Thamodaran & Bruce, 2016). In the latest of these studies, phospho-proteomic mass spectrometry screens of maturing blastocysts (E3.5-E4.5) cultured under control (DMSO) or p38-MAPK inhibitor (SB220025) conditions were employed to identify differentially phosphorylated and thus, candidate p38-MAPK substrates/effectors (Bora et al., 2020). As part of these studies, a phospho-peptide mapping to the DDX21 protein was identified as being depleted under p38-MAPK inhibition conditions (phosphorylation at serine-218). It was also discovered, in the wider context of this study, p38-MAPK activity is required during an early blastocyst window to facilitate general protein translation and rRNA processing necessary to specifically prime subsequent PrE differentiation. As stated in the introduction, DDX21 has been implicated rRNA and ribosome biogenesis (Calo et al., 2015; Fuller-Pace, 2006; Romanova et al., 2009) and it was also confirmed a known DDX21 interactor called MYBPP1A acts to facilitate PrE specification and differentiation in mouse blastocyst ICM (Bora et al., 2020). Therefore, it was decided to investigate DDX21 expression, using immuno-fluorescence based confocal microscopy, in the mouse blastocyst, under both control (DMSO) and p38-MAPK inhibited (SB220025) conditions in more detail. Additionally, we also decided to assay the expression of Nucleostemin (NS also known as Guanine nucleotide-binding protein-like 3 (GNL3)) protein, as it has been reported as functionally related to DDX21(Romanova et al., 2009). As can be seen in Figure 14, both DDX21 and NS are expressed in control treated E4.5 stage blastocysts, with DDX21 appearing more localised to nucleolar structures and NS more generally in the nucleoplasm; although there was some partial co-localization in the nucleoli of ICM cells. Additionally, NS expression seemed higher in ICM cells, with DDX21 levels being more evenly distributed. Quantitation of the nuclear fluorescence intensities (expressed in CTCF, corrected total cell fluorescence, units) of all cells in each channel (*i.e.* NS and DDX21) indeed revealed significantly elevated NS expression in control E4.5 blastocyst inner cells versus outer cells (41205 versus 30889 CTCF units, respectively – Figure 16). A similar quantitative analysis of DDX21 levels revealed an inverse correlation, with comparatively higher levels in outer cells versus inner cells (47503 versus 39400 CTCF units, respectively – Figure 17; cofounding the original visual inspection and highlighting the importance of quantitation.

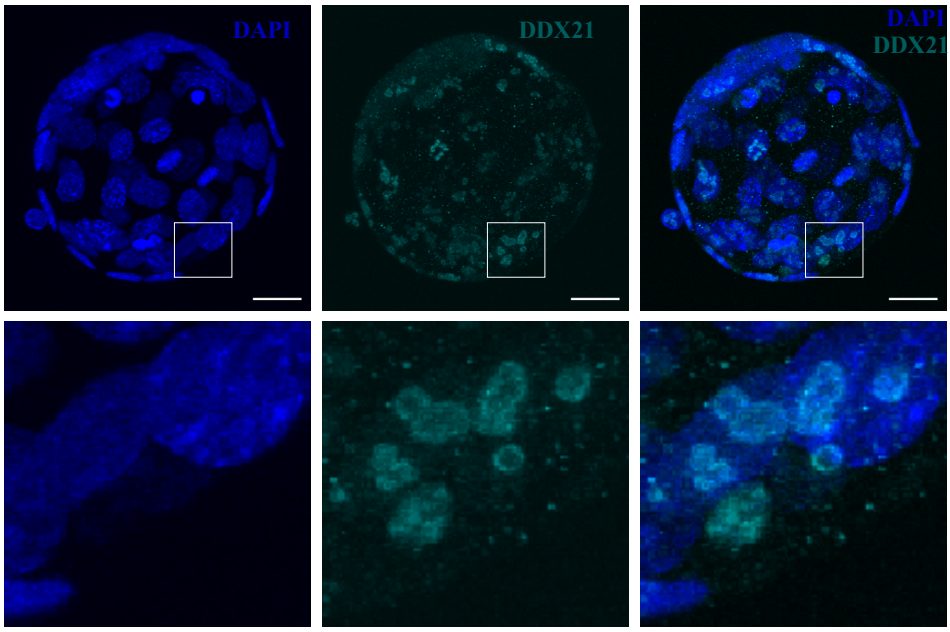

Figure 14: Representative 3D-projection confocal images of blastocysts treated (between E3.5-E4.5) with DMSO control, fixed and immuno-fluorescently stained for DDX21 (cyan) at E4.5. DNA DAPI counterstain (blue) is shown in merged image. Magnified inlays highlight nucleolar co-localization of DDX21; scale bar represents 20µm.

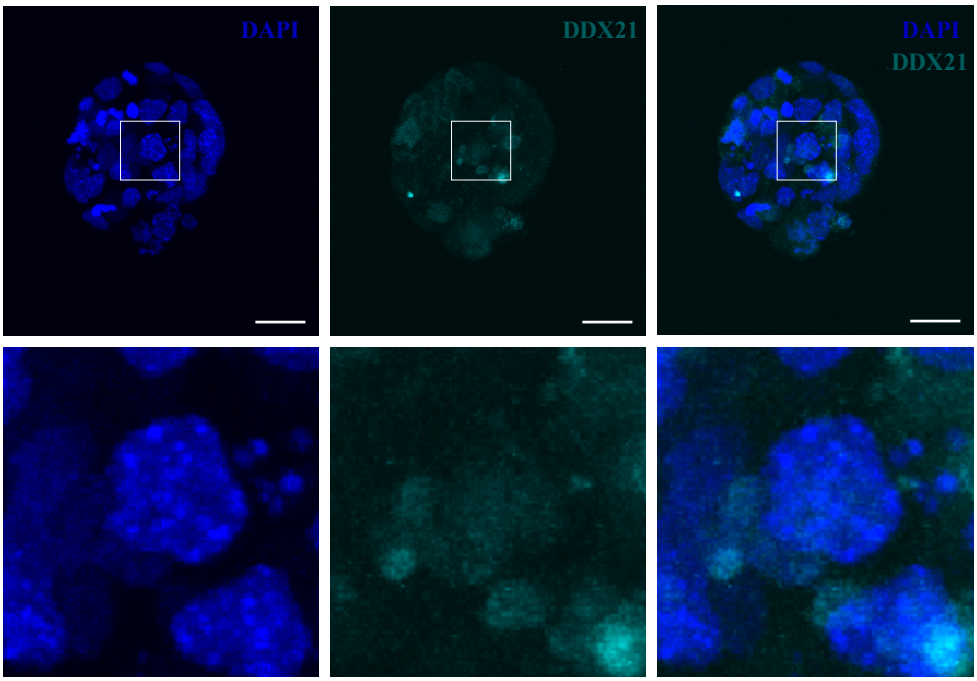

Figure 15: Representative 3D-projection confocal images of blastocysts treated (between E3.5-E4.5) with SB220025 p38-MAPK inhibitor, fixed and immuno-fluorescently stained for DDX21 (cyan) at E4.5. DNA DAPI counterstain (blue) is shown in merged image. Magnified analysis highlights nucleoplasm localization of DDX21; scale bar represents 20µm.

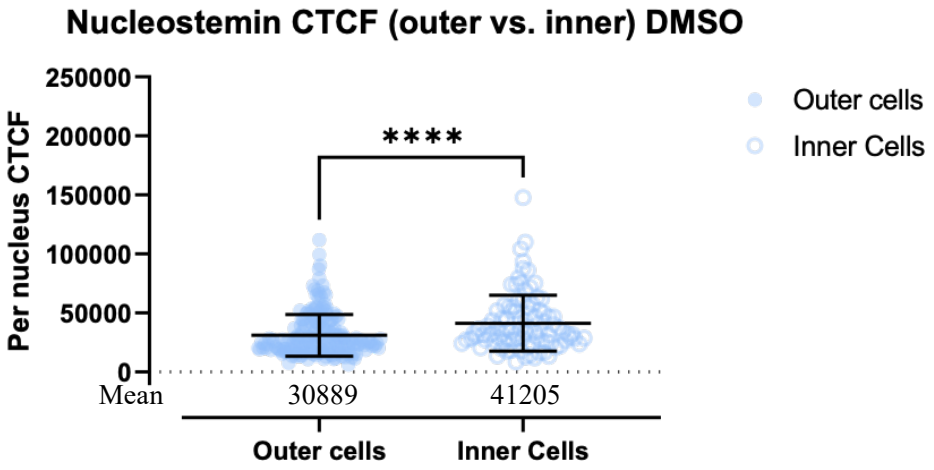

Figure 16: Graph showing comparison of the expression of Nucleostemin in the inner and the outer cells of the control E4.5 stage embryos. The graph also shows the average CTCF expression values of inner and outer cells. Errors are represented as standard deviations and statistical Mann-Whitney test was used; p-value stated (<0.0001) ****. DMSO from n=7 embryos (outer cells=205, inner cells=97).

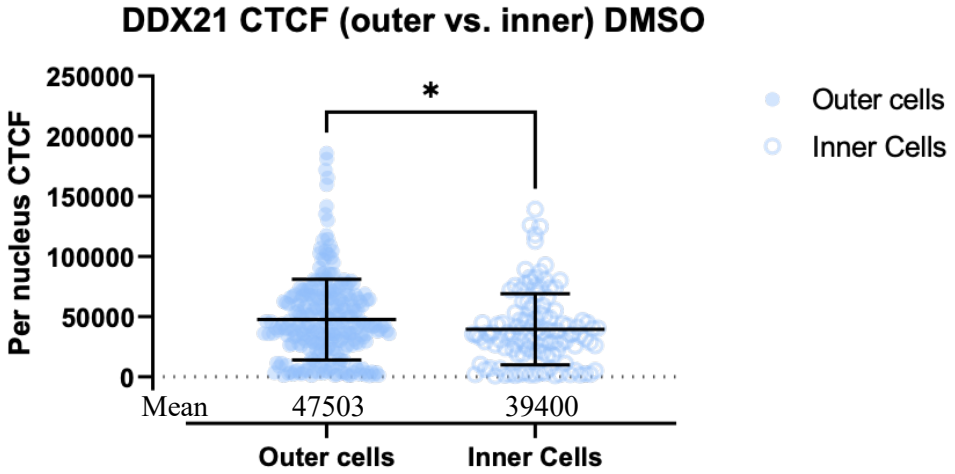

Figure 17: Graph showing comparison of the expression of DDX21 in the inner and the outer cells of the control E4.5 stage embryos. The graph also shows the average CTCF expression values of inner and outer cells. Errors are represented as standard deviations and statistical unpaired t-test was used; p-value stated (0.0223) ns. DMSO from n=16 embryos (outer cells=271, inner cells=122).

We next compared the NS and DDX21 immuno-fluorescent staining obtained under p38-MAPK inhibited conditions with the control treatment. Visual inspection of the acquired confocal micrographs indicated a clear reduction in overall NS staining and a marginal effect on DDX21, after p38-MAPK inhibition (Figure 15). After quantification, the mean CTCF values obtained revealed NS levels were significantly reduced in both outer (16587 versus 30889 CTCF units – Figure 18) and inner (1113 versus 41205 CTCF units – Figure 20 cells after p38-MAPK inhibition. Moreover, under p38-MAPK inhibited conditions, the nevertheless reduced NS levels were found to be significantly higher in outer (16587 CTCF units) cells versus inner cells (1113 CTCF units - Figure 19). This is the inverse of the situation in DMSO control (Figure 17) and implies NS protein expression is more sensitive to p38-MAPK inhibition in inner rather than outer blastocyst cells.

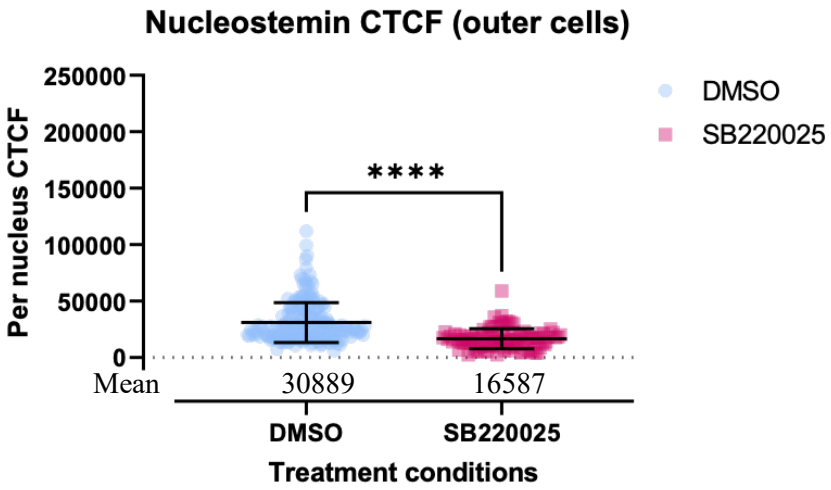

Figure 18: Graph showing comparison of the expression of Nucleostemin in the outer cells of the control (DMSO) treated and p38-MAPK inhibited (SB220025) E4.5 stage embryos. The graph also shows the average CTCF value of outer cell Nucleostemin expression. Errors are represented as standard deviations and statistical Mann-Whitney test was used; p-value stated (<0.0001) ****. DMSO from n=7 embryos (outer cells=205) & SB220025 from n=5 embryos (outer cells=100).

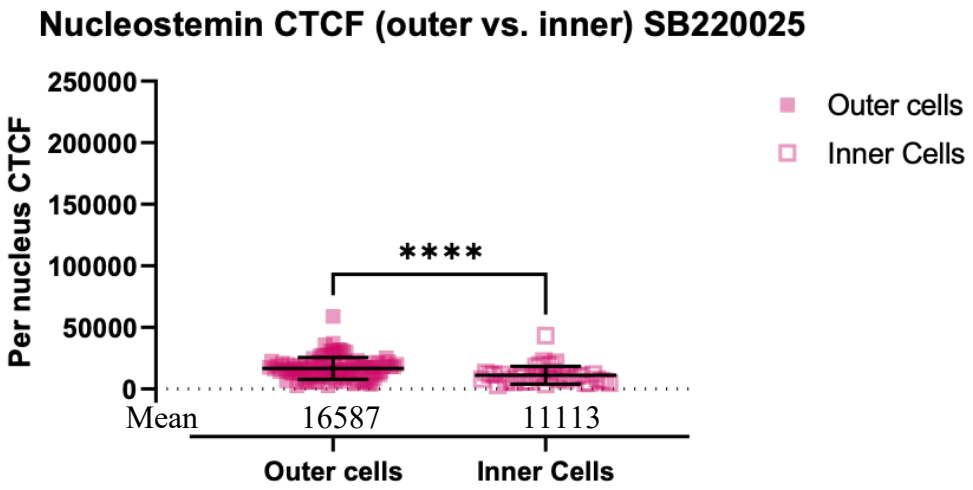

Figure 19: Graph showing comparison of the expression of Nucleostemin in the inner and the outer cells of the p38-MAPK inhibited E4.5 stage embryos. The graph also shows the average CTCF value of inner and outer cell Nucleostemin expression. Errors are represented as standard deviations and statistical Mann-Whitney test was used; p-value stated (0.0001) ****. SB220025 from n=5 embryos (outer cells=100, inner cells=40).

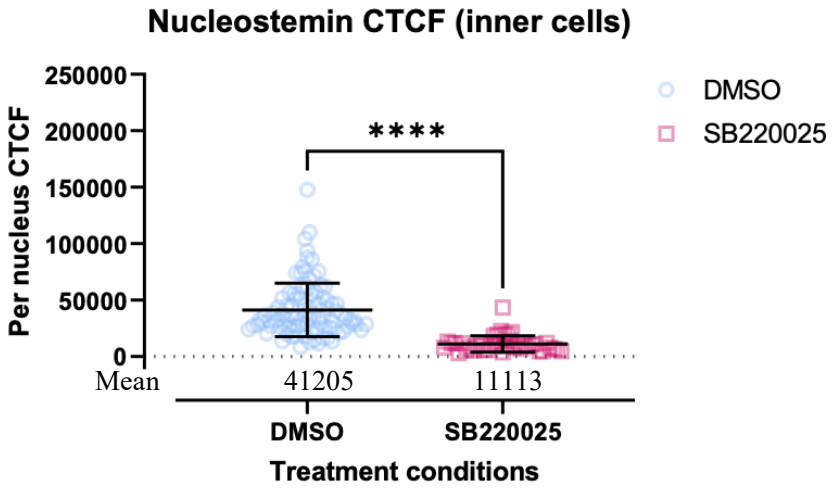

Figure 20: Graph showing comparison of the expression of Nucleostemin in the inner cells of the control (DMSO) treated and p38-MAPK inhibited (SB220025) E4.5 stage embryos. The graph also shows the average CTCF value of inner cell Nucleostemin expression. Errors are represented as standard deviations and statistical Mann-Whitney test was used; p-value stated (0.0001) ****. DMSO from n=7 embryos (inner cells=97) & SB220025 from n=5 embryos (inner cells=40).

In regard to quantified DDX21 levels, p38-MAPK inhibition similarly caused highly significant reductions in expression in both outer (34700 versus 47503 CTCF units- Figure 21) and inner cells (22844 versus 39400 CTCF units - Figure 22) compared to controls. Unlike with NS, the relative overall expression (although reduced compared with controls) remained higher in outer cells (34700 CTCF units) than inner cells (22844 CTCF units - Figure 23); as was the case in control DMSO treated blastocysts at E4.5 (Figure 17). In addition to p38-MAPK inhibition induced reduction in DDX21 protein expression, we also observed a greater propensity for DDX21 to be localised within the nucleoplasm, rather than the robustly nucleolar restricted expression pattern seen in control E4.5 blastocysts (in both inner and outer cells – Figure 15; see also Figure 24). Such altered localisation could potentially indicate a functional regulation of DDX21, that could be related to p38-MAPK directed phosphorylation (as revealed in the original phospho-proteomics screen).

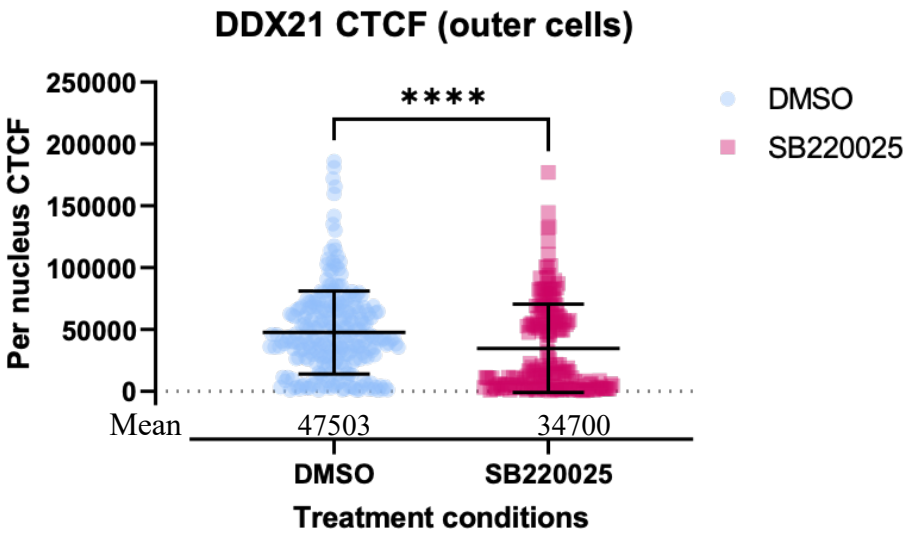

Figure 21: Graph showing comparison of the expression of DDX21 in the outer cells of the control (DMSO) treated and p38-MAPK inhibited (SB220025) E4.5 stage embryos. The graph also shows the average CTCF value of outer cell DDX21 expression. Errors are represented as standard deviations and statistical Mann-Whitney test was used; p-value stated (0.0001) ****. DMSO from n=16 embryos (outer cells=271) & SB220025 from n=15 embryos (outer cells=190).

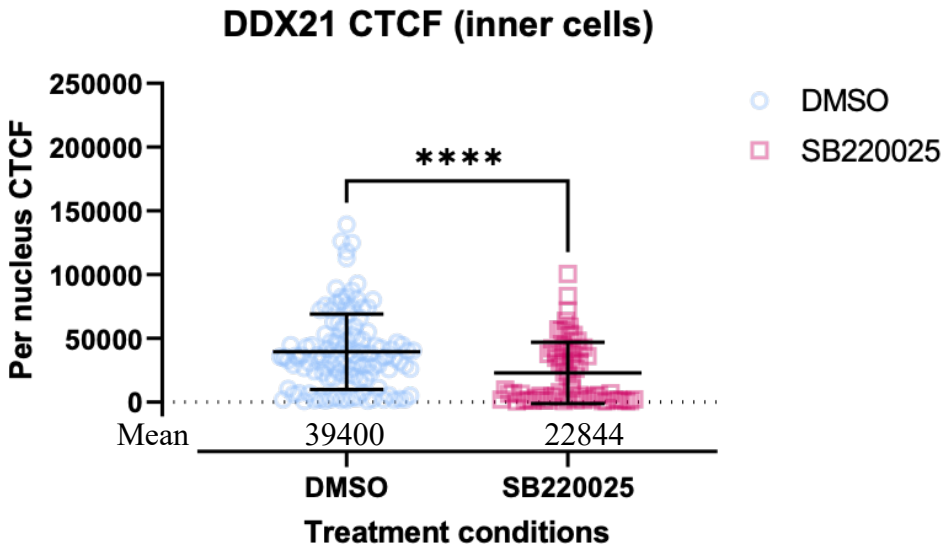

Figure 22: Graph showing comparison of the expression of DDX21 in the inner cells of the control (DMSO) treated and p38-MAPK inhibited (SB220025) E4.5 stage embryos. The graph also shows the average CTCF value of inner cell DDX21 expression. Errors are represented as standard deviations and statistical Mann-Whitney test was used; p-value stated (<0.0001) ****. DMSO from n=16 embryos (inner cells=122) & SB220025 from n=15 embryos (inner cells=67).

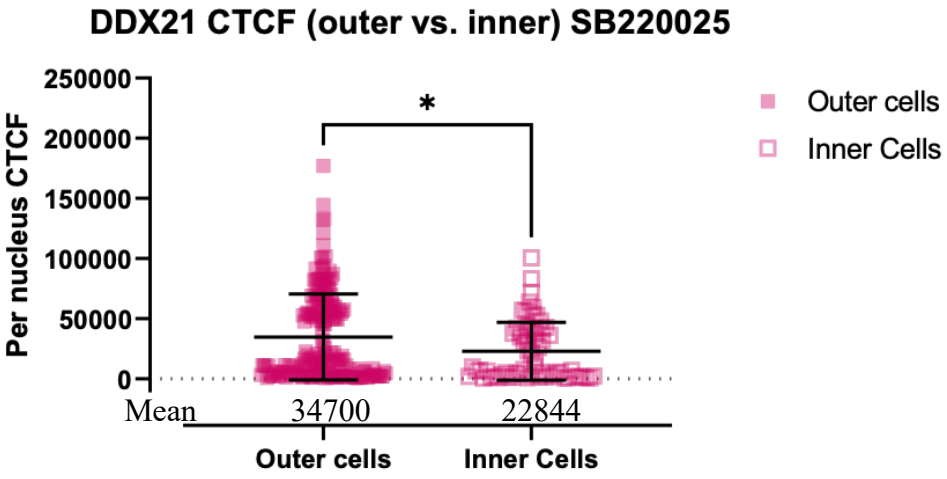

Figure 23: Graph showing comparison of the expression of DDX21 in the inner and the outer cells of the p38-MAPK inhibited E4.5 stage embryos. The graph also shows the average CTCF value of inner and outer cell DDX21 expression. Errors are represented as standard deviations and statistical Mann-Whitney test was used; p-value stated (0.0120) *. SB220025 from n=15 embryos (outer cells=190, inner cells=67).

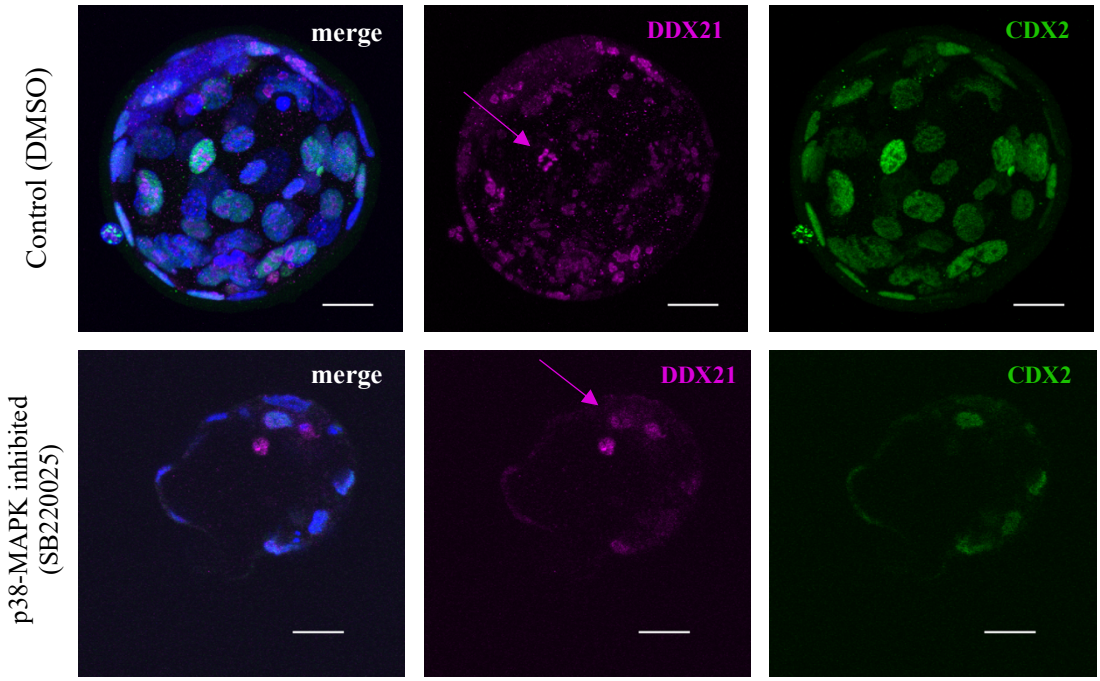

Figure 24: Exemplar projected confocal z-section micrographs of blastocysts treated (between E3.5-E4.5) with DMSO control (upper row) or SB220025 p38-MAPK inhibitor (lower row), fixed and immuno-stained for DDX21 (magneta) and CDX2 (green) at E4.5. DNA DAPI counterstain (blue) is shown in merged image. First arrow (magneta, upper row) highlights nucleolar localization of DDX21 (control) and second arrow (magneta, lower row) highlights nucleoplasm (inhibited) localisation of DDX21. Shown images are from a repeated experiment that included CDX2 to aid identification of outer cells; scale bar represents 20μm.

Overall, this analysis of DDX21 and NS protein expression in control and p38-MAPK inhibitor treated mouse blastocysts confirms expression of both proteins, with partially overlapping expression in cell nucleoli (particularly inner cells). The expression levels of both proteins are sensitive to p38-MAPK activity, with p38-MAPK inhibition (E3.5-E4.5) leading to reduced levels in all cells of the blastocyst (the expression of NS in the ICM is particularly sensitive). Moreover, DDX21 localization switches from an exclusive nucleolar pattern in controls to an increased nucleoplasmic component upon p38-MAPK inhibition (expanded in Figure 24). These data confirm the p38-MAPK sensitivity of the candidate p38-MAPK substrate/effector DDX21 (and functionally related NS) are consistent with the previously uncovered protein translation regulatory role of p38-MAPK during PrE specification (Bora et al., 2020). Note, these results have been incorporated into a manuscript at a currently advanced stage of preparation (Bora et al., 2021 – *manuscript in preparation*).

As described above, we observed that p38-MAPK inhibition during blastocyst maturation caused a relocation of DDX21 protein from an exclusively nucleolar expression pattern to a more general nucleoplasmic one (Figure 24) . In characterizing this phenotype, we had included a co-immuno-fluorescent stain for CDX2 (to better aid inner and outer cell identification). We therefore decided to quantify the expression level of CDX2 to see if it was in anyway sensitive to p38-MAPK inhibition (as was revealed for NS and DDX21 – see above). We found that there was only a marginally significant reduction in CDX2 expression in outer (Figure 25) cells and no difference in inner cell (Figure 26) of control and 38-MAPK inhibitor treated blastocysts (E3.5-E4.5). Although, detectable CDX2 protein levels were drastically and significantly reduced in inner cell versus outer cell populations, irrespective of the control or p38-MAPKi treatment (Figures 27 and 28); reflecting the natural role of CDX2 in the blastocyst TE (Strumpf et al., 2005). These data confirm CDX2 protein expression is not very sensitive to p38-MAPK inhibition during blastocyst maturation and provide a useful negative and reassuring control in relation to the detected reductions in NS and DDX21 protein levels and the DDX21 relocalisation phenotype.

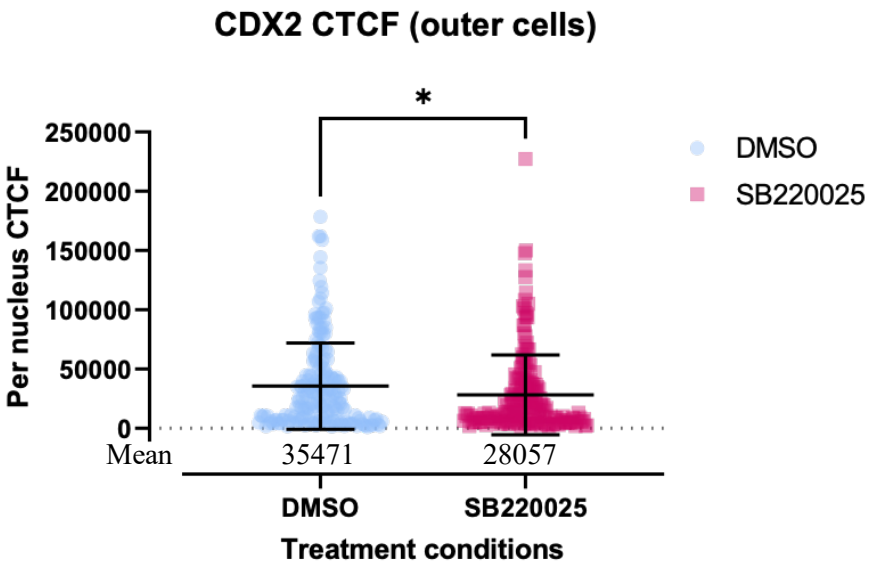

Figure 25: Graph showing comparison of the expression of CDX2 in the outer cells of the control E4.5 stage embryos and inhibited embryos (SB220025). The graph also shows the average CTCF value of outer cell CDX2 expression. Errors are represented as standard deviations and statistical Mann-Whitney test was used; p-value stated (0.0419) *. DMSO from n=9 embryos (outer cells=197) & SB220025 from n=10 embryos (outer cells=191).

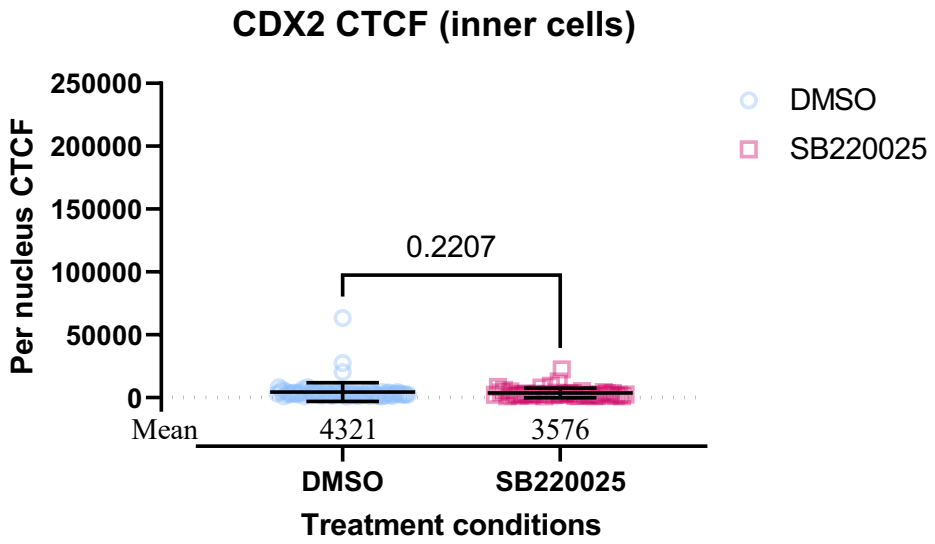

Figure 26: Graph showing comparison of the expression of CDX2 in the inner cells of the control (DMSO) E4.5 stage embryos and inhibited embryos (SB220025). The graph also shows the average CTCF value of inner cell CDX2 expression. Errors are represented as standard deviations and statistical Mann-Whitney test was used; p-value stated (0.2207) ns. DMSO from n=9 embryos (inner cells=81) & SB220025 from n=10 embryos (inner cells=45).

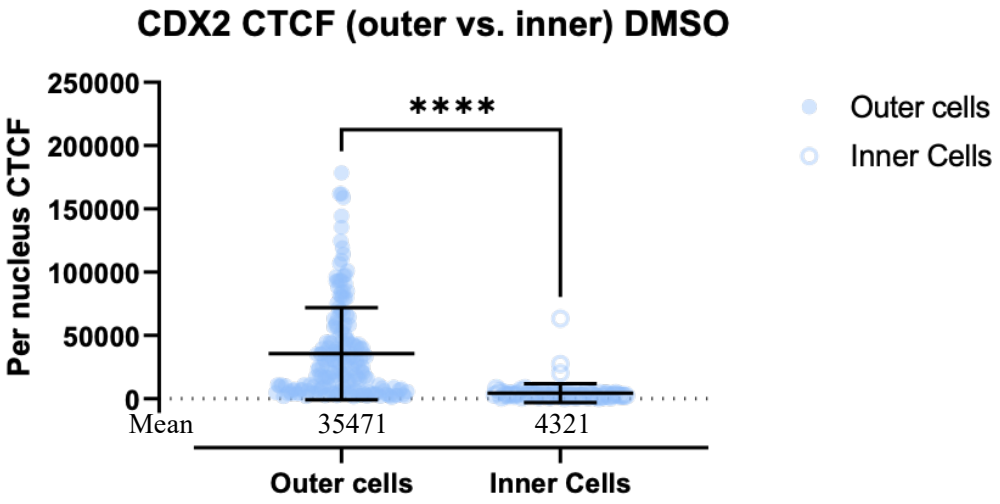

Figure 27: Graph showing comparison of the expression of CDX2 in the inner and the outer cells of the control E4.5 stage embryos. The graph also shows the average CTCF value of inner and outer cell CDX2 expression. Errors are represented as standard deviations and statistical Mann-Whitney test was used; p-value stated (<0.0001) ****. DMSO from n=9 embryos (outer cells=197, inner cells=81).

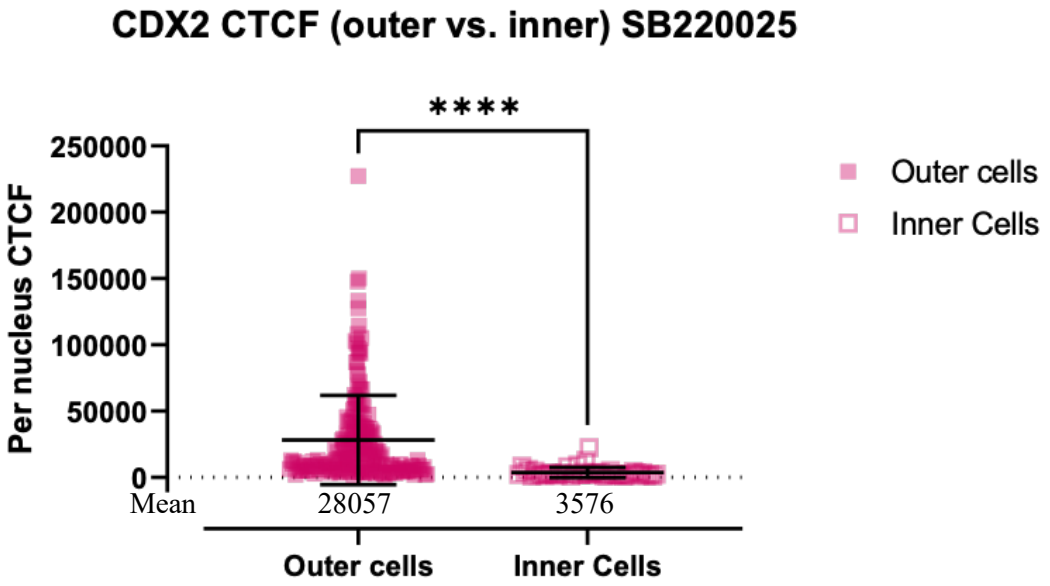

Figure 28: Graph showing comparison of the expression of CDX2 in the inner and the outer cells of the p38-MAPK inhibited E4.5 stage embryos. The graph also shows the average CTCF value of inner and outer cell CDX2 expression. Errors are represented as standard deviations and statistical Mann-Whitney test was used; p-value stated (<0.0001) ****. SB220025 from n=10 embryos (outer cells=191, inner cells=45).

4.4 *Ddx21* downregulation also results in smaller blastocysts and anomalous cell-fate specification

As described above, our laboratory has recently reported p38-MAPK inhibition during blastocyst maturation (E3.5-E4.5) causes blastocyst cavity expansion defects (see data in section 4.1– this data was included in the described manuscript) (Bora et al., 2020). In the preparation of the current DDX21-related manuscript, we therefore hypothesized RNAi mediated knockdown of *Ddx21* expression in developing mouse preimplantation embryo would cause similar cavity expansion defects. Hence, cavity volumes were measured in late blastocysts (E4.5) that were derived from cultured 2-cell (E1.5) stage mouse embryos that had been microinjected with either non-specific control or *Ddx21* specific siRNA in one blastomere (plus histone H2B-RFP mRNA - to create a marked clone of cells comprising 50% of the developing embryo). Efficacy of the *Ddx21* knockdown and the inability of the marked knockdown clones to contribute to PrE was confirmed (Bora et al., 2021 - *unpublished observations in preparation*). As can be clearly seen in Figure 29, the blastocyst volumes of clonally downregulated *Ddx21* blastocysts were >50% smaller than control embryos (300.2 pL versus 606.9 pL), thus confirming our hypothesis. Note, these results have been incorporated into a manuscript at a currently advanced stage of preparation (Bora et al., 2021 – *manuscript in preparation*).

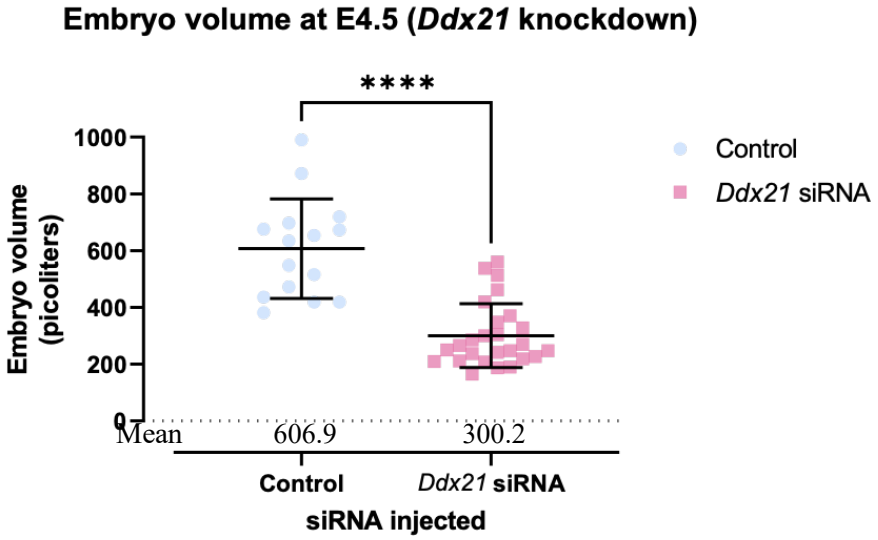

Figure 29: Graph describing the difference in blastocyst volume (E4.5) of control (n=15) treated and clonal *Ddx21* knockdown (n=26) embryos. The graph also shows the mean embryo volume (pL) values. Errors are represented as standard deviations and statistical Mann-Whitney test was used; p-value stated (<0.0001) ****.

4.5 Clonal downregulation of *Tead4*, a TE specific transcription factor, also results in smaller blastocysts

In a similar experiment as that described above for *Ddx21* clonal RNAi-mediated knockdown and blastocyst cavity expansion (section 4.4), 2-cell stage embryos were microinjected in one blastomere at the 2-cell (E1.5) stage with *Tead4* siRNA (plus histone H2B-RFP mRNA). Previous work from our laboratory shows this siRNA is highly efficacious in silencing *Tead4* expression in the developing mouse embryo and moreover marked *Tead4* knockdown clones do not readily contribute to the PrE (Mihajlović & Bruce, 2016). Therefore, given the PrE defect and the fact expanding cavity volume has recently been correlated with PrE specification (Ryan et al., 2019), we hypothesized resulting clonally down-regulated *Tead4* blastocysts may have smaller cavities than control siRNA microinjected blastocysts. As can be seen in Figure 30, this hypothesis was rejected as there was no significant difference in embryo volume between the two groups. This suggests the reduced contribution of marked *Tead4* knockdown clones to PrE is most likely to be cell-autonomous and not influenced by cavity expansion. Remarkably, it also confirms loss of TE specification (as previously observed and confirmed in the *Tead4* knockdown clone) in 50% of the developing preimplantation embryo cells is not sufficient to cause cavity defects (Mihajlović & Bruce, 2016).

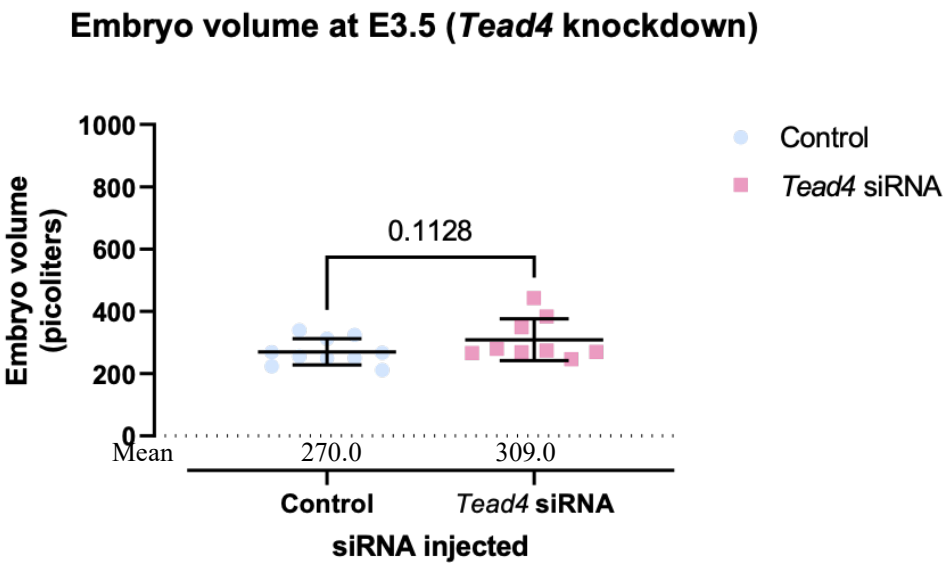

Figure 30: Graph describing the difference in blastocyst (E4.5) of control (n=10) treated condition and clonal *Tead4* knockdown (n=9) embryos. The graph also shows the mean embryo volume values and errors are standard deviations. Mann-Whitney test was used as statistical analysis; p-value stated (0.1128) ns.

5 Discussion

The first aim of this bachelor's thesis was to measure and compare blastocoel cavity volume of control and p38-MAPK inhibitor treated mouse blastocysts. Secondly, we wanted to assay and quantify the expression of potential p38-MAPK effectors (NS and DDX21) during blastocyst maturation, with and without p38-MAPK inhibition. Further, we set out to measure and compared blastocyst cavity volumes upon knockdown of the p38-MAPK effector *Ddx21* and the TE specifying transcription factor *Tead4*.

In previous papers, our laboratory has identified p38-MAPK to be involved in early embryonic development and in particular PrE specification during mouse blastocyst maturation (Bora et al., 2019; Bora et al., 2020; Thamodaran & Bruce, 2016). This result was confirmed by recapitulation in the first section of this thesis, wherein a decrease in GATA4 expressing PrE cells upon p38-MAPKi between E3.5 and E4.5 was observed (Figure 10). Moreover, these same embryos were then used to quantitatively verify p38-MAPK inhibited blastocyst (E3.5-E4.5) have statistically significantly smaller cavities (Figure 13), as was noted (but not quantified) in another of our previous studies (Bora et al., 2019). These data have been included in our laboratory's most recent manuscript submission (Bora et al., 2020 - available as a preprint but also in the latter stages of review at the journal *Communications Biology*). Previous papers from other laboratories have found p38-MAPK inhibition capable of influencing the expression of proteins involved the filling of the blastocoel cavity (Bell & Watson, 2013). In our recent work (Bora et al., 2020), we also report that those same genes are transcriptionally and translationally downregulated under p38-MAPKi, thus possibly explaining why the cavity cannot be filled properly. It is also significant that a group recently reported a positive correlation between expanding blastocyst cavity size and ICM lineage specification and segregation, particularly effecting the PrE (Ryan et al., 2019). The fact p38-MAPK inhibition during blastocyst maturation is associated with smaller cavity size, suggests part of the p38-MAPK inhibition PrE phenotype described in our laboratory (Bora et al., 2019, 2020; Thamodaran & Bruce, 2016) could have its origin in regulation of the expanding blastocoel. However, the recent mechanistic work of our groups strongly suggests there are also strong ICM PrE progenitor cell autonomous effects, related to discreet regulation of translation (Bora et al., 2020).

In our recent work (Bora et al., 2020), a mass spectrometry approach was used to identify candidate proteins that can are phosphorylated by p38-MAPK, and thus could be functionally modified, during blastocyst maturation. This analysis identified proteins involved in protein translation regulation, such as the rRNA processing protein MYBBP1A, that we

went to functionally verify as participating in blastocyst ICM lineage segregation (Bora et al., 2020). Another such protein, although not functionally verified in the same study, was DDX21. As stated in the *Introduction*, DDX21 has been implicated in regulating ribosome biogenesis, via regulation of both rRNA and ribosomal protein encoding mRNAs (Calo et al., 2015; Fuller-Pace, 2006; Romanova et al., 2009). To our knowledge there are no existing studies on the role of DDX21 in preimplantation development, let alone blastocyst ICM lineage derivation. However, the fact we have uncovered a protein translation regulatory role of p38-MAPK during early blastocyst maturation, that is required to prime PrE specification and differentiation (Bora et al., 2020), would certainly be consistent with a potential p38-MAPK regulatory role of DDX21 function. Indeed, in our manuscript currently in the advanced stages of preparation, we describe the expression pattern of DDX21 throughout preimplantation mouse embryo development and confirm that both DDX21 and NS protein levels are sensitive to p38-MAPK inhibition during blastocyst maturation (figures 14-24), with DDX21 localisation changing from an exclusively nucleolar (the site of rRNA synthesis) to a more nucleoplasmic pattern (note, these are the same experiments and analyses described in this thesis). Hence, it seems highly probable that DDX21 (and possibly NS) act as a p38-MAPK sensitive effector in the protein translational regulatory role, that underpins blastocyst ICM PrE specification and differentiation, we have identified (Bora et al., 2020). This is reinforced by the observations we have also made, in the manuscript under preparation, that clonal RNAi-mediated down-regulation of *Ddx2* expression impairs PrE formation in the maturing blastocyst ICM (*our unpublished observations*). The same clonal *Ddx21* downregulation also resulted in smaller blastocyst cavities by the late blastocyst (E4.5) stage (figure 29 – results also included in the manuscript currently under preparation). This is a further validation of the relationship between p38-MAPK and DDX21, and their role in preimplantation embryonic development, as p38-MAPK inhibition too results in smaller blastocysts, as reported in this thesis and included in our resultant publication (Bora et al., 2020). Moreover, these results resonate with those findings that expanding blastocyst cavities positively correlated with appropriate ICM specification and PrE differentiation (Ryan et al., 2019); thus, contributing to an emerging coherent narrative of p38-MAPK function during mouse blastocyst maturation.

6 Conclusion

The study of the role of p38 mitogen activated protein kinases (p38-MAPK) and its effectors in mouse blastocyst maturation and ICM lineage specification (particularly PrE) is still an unfinished work (Bora et al., 2019, 2020; Thamodaran & Bruce, 2016). Here we have contributed by confirming p38-MAPK inhibition is associated with ICM cell fate defects, specifically effecting PrE, and impaired blastocyst cavity expansion (agreeing with recently published literature functionally correlating these two processes). Moreover, that the protein expression levels and sub-nuclear localisation of an empirically identified candidate blastocyst p38-MAPK substrate/effector (DDX21, plus NS), with known roles in ribosome biogenesis and protein regulation, is sensitive to p38-MAPK activity during this same PrE critical blastocyst developmental window. Thus, the data add to the emerging picture of p38-MAPK mediated regulation of blastocyst stage protein translation, required to prime PrE specification and formation (Bora et al., 2020). Moreover, these data have contributed to two manuscripts (one available as a preprint and the other in preparation) that serve to fulfil this greater understanding.

7 References

Bell, C. E., & Watson, A. J. (2013). p38 MAPK Regulates Cavitation and Tight Junction Function in the Mouse Blastocyst. *PLoS ONE*, *8*(4), e59528. https://doi.org/10.1371/journal.pone.0059528

Benos, D. J., Biggers, J. D., Balaban, R. S., Mills, J. W., & Overström, E. W. (1985). Developmental aspects of sodium-dependent transport processes of preimplantation rabbit embryos. *Society of General Physiologists Series*, *39*, 211–235.

Bessonnard, S., Mot, L. De, Gonze, D., Barriol, M., Dennis, C., Goldbeter, A., Dupont, G., & Chazaud, C. (2014). Gata6, Nanog and Erk signaling control cell fate in the inner cell mass through a tristable regulatory network. *Development (Cambridge)*, *141*(19), 3637–3648. https://doi.org/10.1242/dev.109678

Bessonnard, S., Vandormael-Pournin, S., Coqueran, S., Cohen-Tannoudji, M., & Artus, J. (2019). PDGF Signaling in Primitive Endoderm Cell Survival Is Mediated by PI3K-mTOR Through p53-Independent Mechanism. *Stem Cells*, *37*(7), 888–898. https://doi.org/10.1002/stem.3008

Bora, P., Gahurova, L., Mašek, T., Hauserova, A., Potěšil, D., Jansova, D., Susor, A., Zdráhal, Z., Ajduk, A., Pospíšek, M., & Bruce, A. W. (2020). p38-MAPK mediated rRNA processing and translation regulation enables PrE differentiation during mouse blastocyst maturation. *BioRxiv*, 2020.11.30.403931. https://doi.org/10.1101/2020.11.30.403931

Bora, P., Thamodaran, V., Šušor, A., & Bruce, A. W. (2019). p38-Mitogen Activated Kinases Mediate a Developmental Regulatory Response to Amino Acid Depletion and Associated Oxidative Stress in Mouse Blastocyst Embryos. *Frontiers in Cell and Developmental Biology*, *7*(November), 276. https://doi.org/10.3389/fcell.2019.00276

Boroviak, T., Loos, R., Lombard, P., Okahara, J., Behr, R., Sasaki, E., Nichols, J., Smith, A., & Bertone, P. (2015). Lineage-Specific Profiling Delineates the Emergence and Progression of Naive Pluripotency in Mammalian Embryogenesis. *Developmental Cell*, *35*(3), 366–382. https://doi.org/10.1016/j.devcel.2015.10.011

Bury, L., Coelho, P. A., Simeone, A., Ferries, S., Eyers, C. E., Eyers, P. A., Zernicka-Goetz, M., & Glover, D. M. (2017). Plk4 and Aurora A cooperate in the initiation of acentriolar spindle assembly in mammalian oocytes. *The Journal of Cell Biology*, *216*(11), 3571–3590. https://doi.org/10.1083/jcb.201606077

Calo, E., Flynn, R. A., Martin, L., Spitale, R. C., Chang, H. Y., & Wysocka, J. (2015). RNA helicase DDX21 coordinates transcription and ribosomal RNA processing. *Nature*, *518*(7538), 249–253. https://doi.org/10.1038/nature13923

Casser, E., Israel, S., Witten, A., Schulte, K., Schlatt, S., Nordhoff, V., & Boiani, M. (2017). Totipotency segregates between the sister blastomeres of two-cell stage mouse embryos. *Scientific Reports*, *7*(1), 1–15. https://doi.org/10.1038/s41598-017-08266-6

Chaigne, A., Campillo, C., Gov, N. S., Voituriez, R., Azoury, J., Umaña-Diaz, C., Almonacid, M., Queguiner, I., Nassoy, P., Sykes, C., Verlhac, M.-H., & Terret, M.-E. (2013). A soft cortex is essential for asymmetric spindle positioning in mouse oocytes.

Nature Cell Biology, *15*(8), 958–966. https://doi.org/10.1038/ncb2799

Chazaud, C., & Yamanaka, Y. (2016). Lineage specification in the mouse preimplantation embryo. *Development*, *143*(7), 1063–1074. https://doi.org/10.1242/dev.128314

Cockburn, K., & Rossant, J. (2010). Making the blastocyst: lessons from the mouse. *The Journal of Clinical Investigation*, *120*(4), 995–1003. https://doi.org/10.1172/JCI41229

Cuadrado, A., & Nebreda, A. R. (2010). Mechanisms and functions of p38 MAPK signalling. *Biochemical Journal*, *429*(3), 403–417. https://doi.org/10.1042/BJ20100323

Deng, H., Wang, W., Yu, J., Zheng, Y., Qing, Y., & Pan, D. (2015). Spectrin regulates Hippo signaling by modulating cortical actomyosin activity. *ELife*, *4*, e06567. https://doi.org/10.7554/eLife.06567

Eckersley-Maslin, M. A., Alda-Catalinas, C., & Reik, W. (2018). Dynamics of the epigenetic landscape during the maternal-to-zygotic transition. *Nature Reviews. Molecular Cell Biology*, *19*(7), 436–450. https://doi.org/10.1038/s41580-018-0008-z

Frankenberg, S., Gerbe, F., Bessonnard, S., Belville, C., Pouchin, P., Bardot, O., & Chazaud, C. (2011). Primitive Endoderm Differentiates via a Three-Step Mechanism Involving Nanog and RTK Signaling. *Developmental Cell*, *21*(6), 1005–1013. https://doi.org/10.1016/j.devcel.2011.10.019

Fuller-Pace, F. V. (2006). DExD/H box RNA helicases: multifunctional proteins with important roles in transcriptional regulation. *Nucleic Acids Research*, *34*(15), 4206–4215. https://doi.org/10.1093/nar/gkl460

Giannatselis, H., Calder, M., & Watson, A. J. (2011). Ouabain stimulates a Na +/K +-ATPase-mediated SFK-activated signalling pathway that regulates tight junction function in the mouse blastocyst. *PLoS ONE*, *6*(8). https://doi.org/10.1371/journal.pone.0023704

Guo, G., Huss, M., Tong, G. Q., Wang, C., Li Sun, L., Clarke, N. D., & Robson, P. (2010). Resolution of Cell Fate Decisions Revealed by Single-Cell Gene Expression Analysis from Zygote to Blastocyst. *Developmental Cell*, *18*(4), 675–685. https://doi.org/10.1016/j.devcel.2010.02.012

Hirate, Y., Hirahara, S., Inoue, K.-I., Suzuki, A., Alarcon, V. B., Akimoto, K., Hirai, T., Hara, T., Adachi, M., Chida, K., Ohno, S., Marikawa, Y., Nakao, K., Shimono, A., & Sasaki, H. (2013). Polarity-dependent distribution of angiomotin localizes Hippo signaling in preimplantation embryos. *Current Biology : CB*, *23*(13), 1181–1194. https://doi.org/10.1016/j.cub.2013.05.014

Hyafil, F., Morello, D., Babinet, C., & Jacob, F. (1980). A cell surface glycoprotein involved in the compaction of embryonal carcinoma cells and cleavage stage embryos. *Cell*, *21*(3), 927–934. https://doi.org/10.1016/0092-8674(80)90456-0

Ishiuchi, T., & Torres-Padilla, M. E. (2013). Towards an understanding of the regulatory mechanisms of totipotency. *Current Opinion in Genetics and Development*, *23*(5), 512–518. https://doi.org/10.1016/j.gde.2013.06.006

Kang, M., Piliszek, A., Artus, J., & Hadjantonakis, A.-K. (2013). FGF4 is required for lineage restriction and salt-and-pepper distribution of primitive endoderm factors but not their initial expression in the mouse. *Development*, *140*(2), 267–279. https://doi.org/10.1242/dev.084996

Kang, Minjung, Garg, V., & Hadjantonakis, A. (2017). Lineage Establishment and Progression within the Inner Cell Mass of the Mouse Blastocyst Requires FGFR1 and FGFR2. *Developmental Cell*, *41*(5), 496-510.e5. https://doi.org/10.1016/j.devcel.2017.05.003

Larue, L., Ohsugi, M., Hirchenhain, J., & Kemler, R. (1994). Trophectoderm Epithelium. *Developmental Biology*, *91*(August), 8263–8267.

Li, L., Lu, X., & Dean, J. (2013). The maternal to zygotic transition in mammals. *Molecular Aspects of Medicine*, *34*(5), 919–938. https://doi.org/10.1016/j.mam.2013.01.003

Marikawa, Y., & Alarcon, V. B. (2012). Creation of trophectoderm, the first epithelium, in mouse preimplantation development. *Results and Problems in Cell Differentiation*, *55*, 165–184. https://doi.org/10.1007/978-3-642-30406-4_9

McCloy, R. A., Rogers, S., Caldon, C. E., Lorca, T., Castro, A., & Burgess, A. (2014). Partial inhibition of Cdk1 in G 2 phase overrides the SAC and decouples mitotic events. *Cell Cycle*, *13*(9), 1400–1412. https://doi.org/10.4161/cc.28401

McLaren, A., & Smith, R. (1977). Functional test of tight junctions in the mouse blastocyst. *Nature*, *267*(5609), 351–353. https://doi.org/10.1038/267351a0

Menchero, S., Rayon, T., Andreu, M. J., & Manzanares, M. (2017). Signaling pathways in mammalian preimplantation development: Linking cellular phenotypes to lineage decisions. *Developmental Dynamics*, *246*(4), 245–261. https://doi.org/10.1002/dvdy.24471

Mihajlović, A. I., & Bruce, A. W. (2016). Rho-associated protein kinase regulates subcellular localisation of Angiomotin and Hippo-signalling during preimplantation mouse embryo development. *Reproductive Biomedicine Online*, *33*(3), 381–390. https://doi.org/10.1016/j.rbmo.2016.06.028

Mihajlović, A. I., & Bruce, A. W. (2017). The first cell-fate decision of mouse preimplantation embryo development: integrating cell position and polarity. *Open Biology*, *7*(11). https://doi.org/10.1098/rsob.170210

Molotkov, A., Mazot, P., Brewer, J. R., Cinalli, R. M., & Soriano, P. (2017). Distinct Requirements for FGFR1 and FGFR2 in Primitive Endoderm Development and Exit from Pluripotency. *Developmental Cell*, *41*(5), 511-526.e4. https://doi.org/10.1016/j.devcel.2017.05.004

Molotkov, A., & Soriano, P. (2018). Distinct mechanisms for PDGF and FGF signaling in primitive endoderm development. *Developmental Biology*, *442*(1), 155–161. https://doi.org/10.1016/j.ydbio.2018.07.010

Natale, D. R., Paliga, A. J. M., Beier, F., D'Souza, S. J. A., & Watson, A. J. (2004). p38 MAPK signaling during murine preimplantation development. *Developmental Biology*,

268(1), 76–88. https://doi.org/10.1016/j.ydbio.2003.12.011

Ohnishi, Y., Huber, W., Tsumura, A., Kang, M., Xenopoulos, P., Kurimoto, K., Oleś, A. K., Araúzo-Bravo, M. J., Saitou, M., Hadjantonakis, A.-K., & Hiiragi, T. (2014). Cell-to-cell expression variability followed by signal reinforcement progressively segregates early mouse lineages. *Nature Cell Biology*, *16*(1), 27–37. https://doi.org/10.1038/ncb2881

Perona, R. M., & Wassarman, P. M. (1986). Mouse blastocysts hatch in vitro by using a trypsin-like proteinase associated with cells of mural trophectoderm. *Developmental Biology*, *114*(1), 42–52. https://doi.org/10.1016/0012-1606(86)90382-9

Potapova, T. A., Sivakumar, S., Flynn, J. N., Li, R., & Gorbsky, G. J. (2011). Mitotic progression becomes irreversible in prometaphase and collapses when Wee1 and Cdc25 are inhibited. *Molecular Biology of the Cell*, *22*(8), 1191–1206. https://doi.org/10.1091/mbc.E10-07-0599

Remy, G., Risco, A. M., Iñesta-Vaquera, F. A., González-Terán, B., Sabio, G., Davis, R. J., & Cuenda, A. (2010). Differential activation of p38MAPK isoforms by MKK6 and MKK3. *Cellular Signalling*, *22*(4), 660–667. https://doi.org/10.1016/j.cellsig.2009.11.020

Romanova, L., Grand, A., Zhang, L., Rayner, S., Katoku-Kikyo, N., Kellner, S., & Kikyo, N. (2009). Critical role of nucleostemin in pre-rRNA processing. *The Journal of Biological Chemistry*, *284*(8), 4968–4977. https://doi.org/10.1074/jbc.M804594200

Ryan, A. Q., Chan, C. J., Graner, F., & Hiiragi, T. (2019). Lumen Expansion Facilitates Epiblast-Primitive Endoderm Fate Specification during Mouse Blastocyst Formation. *Developmental Cell*, *51*(6), 684-697.e4. https://doi.org/10.1016/j.devcel.2019.10.011

Sasaki, H. (2015). Position- and polarity-dependent Hippo signaling regulates cell fates in preimplantation mouse embryos. *Seminars in Cell and Developmental Biology*, *47–48*, 80–87. https://doi.org/10.1016/j.semcdb.2015.05.003

Sasaki, H. (2017). Roles and regulations of Hippo signaling during preimplantation mouse development. *Development Growth and Differentiation*, *59*(1), 12–20. https://doi.org/10.1111/dgd.12335

Seshagiri, P. B., Sen Roy, S., Sireesha, G., & Rao, R. P. (2009). Cellular and molecular regulation of mammalian blastocyst hatching. *Journal of Reproductive Immunology*, *83*(1–2), 79–84. https://doi.org/10.1016/j.jri.2009.06.264

Shirayoshi, Y., Okada, T. S., & Takeichi, M. (1983). The calcium-dependent cell-cell adhesion system regulates inner cell mass formation and cell surface polarization in early mouse development. *Cell*, *35*(3 Pt 2), 631–638. https://doi.org/10.1016/0092-8674(83)90095-8

Strumpf, D., Mao, C.-A., Yamanaka, Y., Ralston, A., Chawengsaksophak, K., Beck, F., & Rossant, J. (2005). Cdx2 is required for correct cell fate specification and differentiation of trophectoderm in the mouse blastocyst. *Development (Cambridge, England)*, *132*(9), 2093–2102. https://doi.org/10.1242/dev.01801

Tarkowski, A. K. (1959). Experiments on the development of isolated blastomers of mouse

eggs. *Nature*, *184*, 1286–1287. https://doi.org/10.1038/1841286a0

Thamodaran, V., & Bruce, A. W. (2016). p38 (Mapk14/11) occupies a regulatory node governing entry into primitive endoderm differentiation during preimplantation mouse embryo development. *Open Biology*, *6*(9), 15034. https://doi.org/10.1098/rsob.160190

Wang, C., Liu, X., Gao, Y., Yang, L., Li, C., Liu, W., Chen, C., Kou, X., Zhao, Y., Chen, J., Wang, Y., Le, R., Wang, H., Duan, T., Zhang, Y., & Gao, S. (2018). Reprogramming of H3K9me3-dependent heterochromatin during mammalian embryo development. *Nature Cell Biology*, *20*(5), 620–631. https://doi.org/10.1038/s41556-018-0093-4

Wang, H., Ding, T., Brown, N., Yamamoto, Y., Prince, L. S., Reese, J., & Paria, B. C. (2008). Zonula occludens-1 (ZO-1) is involved in morula to blastocyst transformation in the mouse. *Developmental Biology*, *318*(1), 112–125. https://doi.org/10.1016/j.ydbio.2008.03.008

Watson, A. J., & Barcroft, L. C. (2001). Regulation of blastocyst formation. *Frontiers in Bioscience : A Journal and Virtual Library*, *6*, D708-30. https://doi.org/10.2741/watson

White, M. D., Zenker, J., Bissiere, S., & Plachta, N. (2018). Instructions for Assembling the Early Mammalian Embryo. *Developmental Cell*, *45*(6), 667–679. https://doi.org/10.1016/j.devcel.2018.05.013

Wicklow, E., Blij, S., Frum, T., Hirate, Y., Lang, R. A., Sasaki, H., & Ralston, A. (2014). HIPPO Pathway Members Restrict SOX2 to the Inner Cell Mass Where It Promotes ICM Fates in the Mouse Blastocyst. *PLoS Genetics*, *10*(10). https://doi.org/10.1371/journal.pgen.1004618

Yi, K., Unruh, J. R., Deng, M., Slaughter, B. D., Rubinstein, B., & Li, R. (2011). Dynamic maintenance of asymmetric meiotic spindle position through Arp2/3-complex-driven cytoplasmic streaming in mouse oocytes. *Nature Cell Biology*, *13*(10), 1252–1258. https://doi.org/10.1038/ncb2320

Zenker, J., White, M. D., Gasnier, M., Alvarez, Y. D., Lim, H. Y. G., Bissiere, S., Biro, M., & Plachta, N. (2018). Expanding Actin Rings Zipper the Mouse Embryo for Blastocyst Formation. *Cell*, *173*(3), 776-791.e17. https://doi.org/10.1016/j.cell.2018.02.035

Zernicka-Goetz, M., Morris, S. A., & Bruce, A. W. (2009). Making a firm decision: multifaceted regulation of cell fate in the early mouse embryo. *Nature Reviews Genetics*, *10*(7), 467–477. https://doi.org/10.1038/nrg2564

Zhang, B., Zheng, H., Huang, B., Li, W., Xiang, Y., Peng, X., Ming, J., Wu, X., Zhang, Y., Xu, Q., Liu, W., Kou, X., Zhao, Y., He, W., Li, C., Chen, B., Li, Y., Wang, Q., Ma, J., … Xie, W. (2016). Allelic reprogramming of the histone modification H3K4me3 in early mammalian development. *Nature*, *537*(7621), 553–557. https://doi.org/10.1038/nature19361